Stony Brook University

Trace Element Mobility During Acid Aqueous Alteration of Martian Basalt

A Thesis Presented

by

Lauren Jane Beavon

to

The Graduate School

in Partial Fulfillment of the

Requirements

for the Degree of

Master of Science

in

Geosciences

Stony Brook University

May 2010

Stony Brook University

The Graduate School

Lauren Jane Beavon

We, the thesis committee for the

above candidate for the Master of Science degree, hereby recommend

acceptance of this thesis.

Dr. Scott M. McLennan
Thesis Advisor
Professor, Department of Geosciences

Dr. Richard J. Reeder
Chairperson of Defense
Chair and Professor, Department of Geosciences

Dr. Donald H. Lindsley
Distinguished Professor Emeritus
Department of Geosciences

This thesis is accepted by the Graduate School

Lawrence Martin
Dean of the Graduate School

Abstract of the Thesis

Trace Element Mobility During Acid Aqueous Alteration of Martian Basalt

by

Lauren Jane Beavon

Master of Science

in

Geosciences

Stony Brook University

2010

It is widely believed that aqueous alteration on Mars has been strongly influenced by low pH conditions over a considerable fraction of Martian geological history. Previous experimental work demonstrated that these low pH environments result in the mobility of elements, such as Fe(III) and Al, that are relatively insoluble under most near surface conditions on Earth. Although these studies have increased our understanding of major element behavior, little is known about the mobility of trace elements under Martian conditions. A series of aqueous alteration experiments on synthesized Martian basalt, reported in this thesis, allows better understanding of the potential mobility of Ni, Zn, and Cr on the Martian surface. These elements were chosen because of their variability in rocks and soils analyzed on the Martian surface by the Mars Exploration Rovers. Experiments were performed on a starting basalt composition similar to the average composition of the Martian upper crust over a range of pH (0-4) and under varying

degrees of crystallinity (glass and crystalline basalt). Similar experiments were also performed on natural chromites to assess their reactivity and the role this mineral plays in the mobility of Cr. In the basaltic glass experiments Ni was found to be the most mobile element, followed by Cr and then Zn. The mobility of cations in crystalline basalt is dependent on their mineralogical setting. Consequently, Ni was also found to be the most mobile element in the crystalline basalt due to its abundance in olivine, the most susceptible mineral present. During the chromite alteration experiments, chromite was found to dissolve non-stoichiometrically. The reactivity of basalt and chromite with various acidic solutions is such that they could make an important contribution of Ni, Zn and Cr ions to aqueous solutions on the Martian surface. However, the liberation of these elements appears to depend on their coordination within the structure of the material. A cation in a network modifying site will be released into solution more readily than one in a network forming site. This may be influenced by the presence of other cations and their availability to charge balance or compete for that site. Once mobile in Martian solutions, Ni, Zn and Cr may have been available for incorporation into secondary mineral phases, such as sulfates, oxides, chlorides and clays, or adsorption onto their surfaces.

Dedication

I would like to dedicate this thesis to my parents. Without their love, encouragement and guidance I would not be where I am today. I hope I continue to make them proud.

Table of Contents

List of Figures

List of Tables

Acknowledgments

I would like to thank Scott McLennan, my thesis advisor, for all of the support and guidance he has shown me throughout my time here at Stony Brook. I could not have finished this research without his patience and continued reassurance that we would always find a solution to every one of our experimental issues. I would also like to thank Don Lindsley, who has been like a second advisor to me. I cannot thank Don enough for all of his time, knowledge and wisdom. Without him this research would not have been possible and he will always have my deepest gratitude. To my mum, dad and Ria, thank you for always being there and believing in me. And to Dan, there are no words to explain what you mean to me. Thank you for your endless love, encouragement and support.

Chapter 1

Introduction

Understanding surficial processes on Mars is the key to constraining past climatic conditions and the history of aqueous processes. Consequently, much effort has been put into better understanding the Martian surface. Previous missions to Mars including Viking, Pathfinder and Phoenix as well as the presently underway Mars Exploration Rovers (MER) have provided important insight into the past and present conditions on the surface. New mineralogical and chemical data derived from these missions support earlier suggestions that the surface of Mars has been influenced by liquid water throughout much of its geologic history [*Arvidson et al.*, 2006; *Carr*, 1996; *Gellert et al.*, 2004; *Grotzinger et al.*, 2005; *McLennan et al.*, 2005; *Squyres et al.*, 2004; *Squyres and Knoll*, 2005]. High concentrations of sulfur and chlorine have been observed within soils at the landing sites of Viking 1 and 2, Pathfinder, Spirit and Opportunity (Table 1). These enrichments are believed to have been the result, ultimately, of volcanic outgassing of sulfur and chlorine that may have reacted with water vapor to form sulfuric and hydrochloric acids [*Banin et al.*, 1997; *Burns*, 1987; *Gaillard and Scaillet*, 2009]. In addition, a number of sulfate minerals, including the detection of jarosite on the Meridiani Plains and a variety of ferric sulfates in the Columbia Hills (Figure 1a), indicate that much of the fluid alteration has been strongly influenced by low pH conditions [*Gellert et al.*, 2004; *Ming et al.*, 2008; *Morris et al.*, 2006a; *Rieder et al.*,

2004; *Wang et al.*, 2008; *Yen et al.*, 2008]. As a result, Martian rocks and soils have not evolved in a manner comparable to those found on Earth, and it has been suggested that the sulfur cycle, rather than the carbon cycle, has dominated surficial processes during much of the Martian geological history [*McLennan and Grotzinger*, 2008]. Consequently, many Martian studies have focused on the weathering of basalts and the formation of secondary minerals under acidic conditions.

A number of experimental weathering studies have attempted to understand acid weathering in Martian environments [*Baker et al.*, 2000; *Banin et al.*, 1997; *Golden et al.*, 2005; *Hurowitz et al.*, 2005; *Tosca et al.*, 2004]. Many studies have focused on using terrestrial basalt compositions as Martian analogs [*Baker et al.*, 2000; *Banin et al.*, 1997; *Golden et al.*, 2005; *Morris et al.*, 2000a, 2000b]. However, the composition and mineralogy of many common terrestrial basalts are significantly different from those of the most common Martian basalts (Table 2). Some differences in composition, such as silica content, have a profound affect on the reactivity of glass, which influences the composition of weathering solutions and resulting secondary phases [*Bouska*, 1993; *Curti et al.*, 2006; *Glass*, 1984; *Jantzen and Plodinec*, 1984; *Oelkers*, 2001; *Oelkers and Gislason*, 2001; *White*, 1984]. In addition, the Fe-rich nature and common presence of olivine in Martian basalts result in Fe- and Mg-rich fluids when altered and such fluids appear to best explain the nature of known and inferred Martian evaporite mineralogy [*Tosca et al.*, 2004, 2005; *Tosca and McLennan*, 2006]. For these reasons, more recent experimental work has been performed on synthetic Martian basalt compositions to better match the bulk chemistry of the rocks found on the surface of Mars [*Hurowitz et al.*, 2005; *Tosca et al.*, 2004].

Oxides wt %	Spirit Soil Gusev plains	Opportunity Soil Meridiani Planum	Pathfinder Soil Ares Vallis	Viking Soil Chryse soil
SiO_2	45.9	45.5	42.1	47
TiO_2	0.89	1.05	0.87	0.69
Al_2O_3	9.83	9.22	9.5	7.9
FeO_T	16.1	17.9	21.6	17.7
Cr_2O_3	0.31	0.39	0.29	-
MnO	0.32	0.36	0.31	-
MgO	8.33	7.63	7.78	6.5
CaO	6.27	6.68	6.37	6.2
Na_2O	2.98	2.25	2.84	-
K_2O	0.47	0.48	0.6	-
P_2O5	0.86	0.87	0.74	-
SO_3	6.85	6.81	6.27	8.3
Cl	0.82	0.73	0.76	0.85
Total	99.9	99.9	100	-

Table 1. Chemical composition of soils on Mars. Note the high concentrations of sulfur and chlorine in all of these analyses. Spirit and Opportunity data represents an average of four dust-rich soil analyses. Pathfinder and Viking analyses also represent average soils. Data taken from *Taylor and McLennan* [2009].

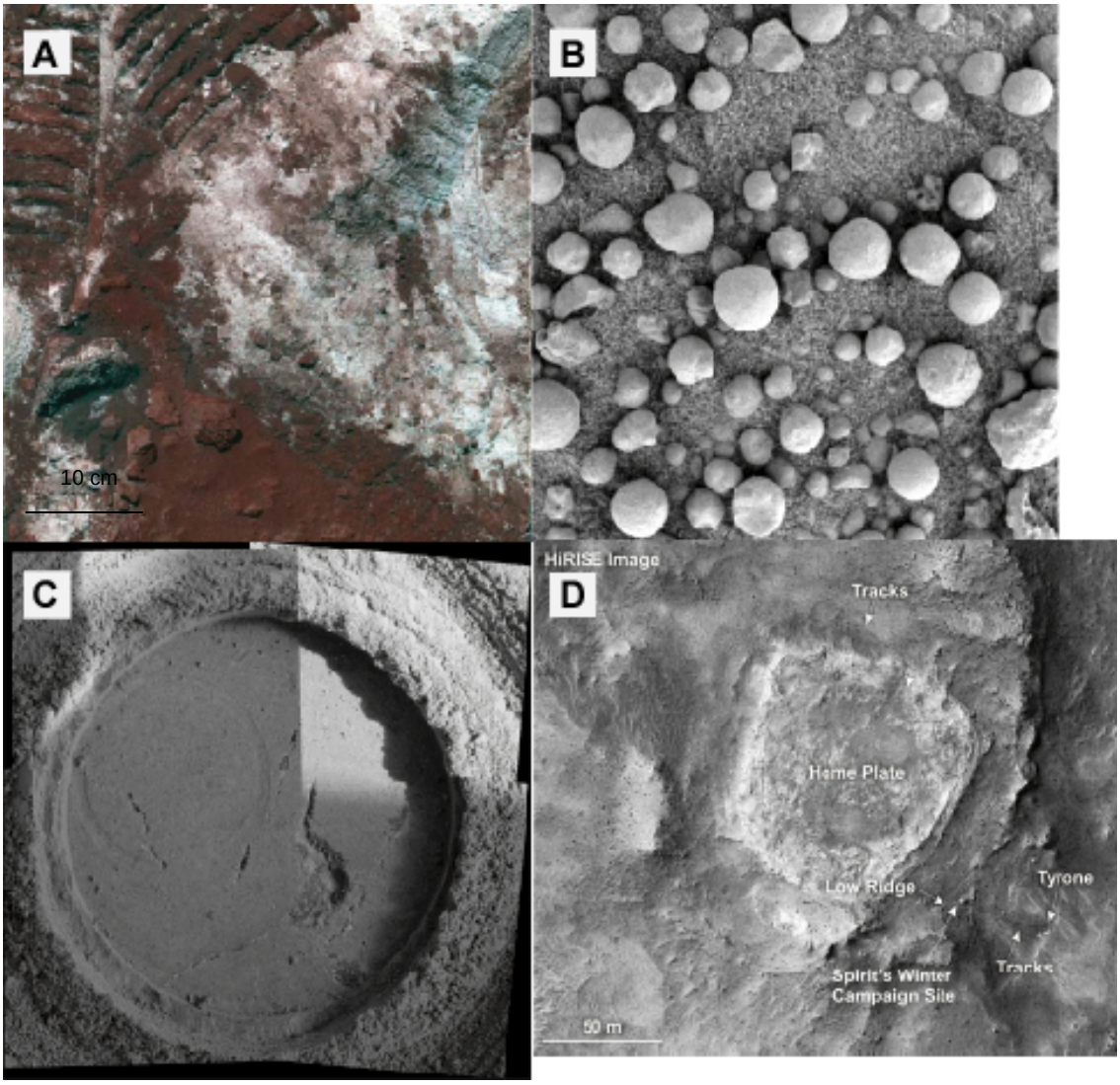

Figure 1. (a) False color Pancam image of Paso Robles class soil. Bright patches were measured to be high in sulfur and the soil is dominated by ferric iron sulfates, silica, and Mg-sulfates [*Yen et al*., 2008]. (b) A picture taken by the microscopic imager near Victoria Crater shows hematitic spherules up to 5 millimeters in diameter. (c) RATed hole on a rock called Uchben in the Columbia Hills (the circle is 4.5 cm in diameter). The Rock Abrasion Tool (RAT) makes in possible to analyze the interior of rocks, which have lower concentrations of S and Cl than the rocks exterior. This indicates that elevated S and Cl is not an intrinsic igneous characteristic. (d) An image of Home Plate taken by the Mars Reconnaissance Orbiter's High Resolution Imaging Science Experiment camera. Images courtesy of NASA.

Acidic alteration studies of synthesized Martian basalts have revealed that solution chemistry is dominated by mineral dissolution rather than by chemical leaching or alteration of primary igneous minerals. Therefore, the difference in primary mineralogy of Martian rocks compared to those found on Earth greatly affects the resulting fluid chemistry. These studies have also shown that low pH environments result in the mobility of elements, such as Fe(III) and Al, that are relatively insoluble under most near surface conditions on Earth [*Hurowitz et al.*, 2006; *Tosca et al.*, 2004]. As dissolved cations influence the types of secondary minerals that are present on the surface (both residual and subsequent evaporation minerals), it is important to understand their behavior. Although the above-mentioned studies have increased our understanding of major element behavior, little is known about the mobility of trace elements under Martian conditions.

The Alpha Particle X-ray Spectrometers aboard the Mars Exploration Rovers are able to determine the concentrations of a number of trace elements in rocks and soils on the surface of Mars, including Cr, Ni, and Zn. These elements, notably Cr and Ni, are important petrogenetic indicators of igneous differentiation processes in basalts and in sedimentary rocks on Earth have been used to evaluate both provenance and weathering processes [*McLennan et al.*, 1993, *Taylor and McLennan*, 1985]. Although the nature of Ni, Zn and Cr on Mars is not fully understood, attempts have been made to utilize these elements to resolve a number of different issues.

One of these issues lies in understanding the origin of basalts found on the Martian surface. Nickel-magnesium and chromium-magnesium ratios have been employed as petrogenetic indicators for picritic basalts found at Gusev Crater and to link

a possible connection between these Gusev basalts and olivine-phyric shergottites [*McSween et al.*, 2006]. Ni also shows a strong enrichment in hematite spherules found at Meridiani Planum [*Burt et al.*, 2008; *Morris et al.*, 2006b; *Yen et al.*, 2005; *Yen et al.*, 2006] (Figure 1b) and in some cases this enrichment has been used to explain their formation [*Knauth et al*., 2005, *Yen et al.*, 2006]. Low abundances of Ni and Cr along with other elements in samples analyzed in the Columbia Hills have been used as signatures to relate different classes of rocks and soils [*Clark et al*., 2006, 2007a]. In a final example, *Schmidt et al.* [2008a, 2008b] have explained the decreasing abundances of Zn and Ni from east to west in the vicinity of Home Plate as a decrease in temperature within a hydrothermal setting (Figure 1d).

Results obtained from the hundreds of analysis performed on altered and unaltered igneous rocks, sedimentary rocks and soils, at both landing sites have shown that the trace elements Ni, Zn, and Cr are highly variable both among different lithologies and within individual lithological types [*Clark et al.*, 2007b; *Gellert et al.*, 2004; *Rieder et al.*, 2004] (Figure 2). The variability of these trace elements generates many questions about the processes that control their distribution. A meteoritic component, on the order of 1% to 3%, might be partly responsible for elevated concentrations of nickel in some soil samples [*Gellert et al.*, 2004; *Yen et al.*, 2006]. Volatile elements such as zinc can be separated from magmas during degassing and be deposited as volcanic condensates [*Aiuppa et al.*, 2000a; *Newsom and Hagerty*, 1997; *Squyres et al.*, 2007; *Yen et al.*, 2005]. On the other hand, aqueous alteration of basalt, especially at low pH, may have mobilized these elements making them available during the formation of evaporates, which on Mars commonly are are Mg- and Fe-rich, and other secondary minerals. Alternatively, if these

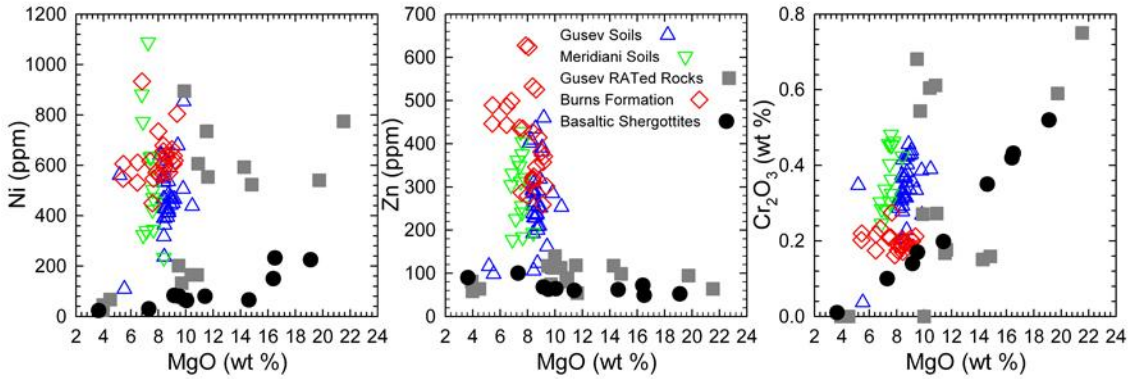

Figure 2. Plots of Ni, Zn and Cr versus MgO for Gusev and Meridiani soils, Gusev RATed rocks, RATed Meridiani outcrop (Burns formation) and basaltic shergottites

elements remain relatively immobile during alteration, it could have resulted in residual enrichments within the altered rock. In this case, if Ni, Zn and Cr are contained predominantly within the siliciclastic components of the sedimentary rocks and soils on Mars, they may provide a useful provenance signature.

In this study we concentrate on a central question to addressing these issues: what is the nature of the mobility of Ni, Zn, and Cr during aqueous alteration under proposed Martian conditions? To accomplish this, we present the results from a series of batch low pH alteration experiments performed on synthetic Martian basalt. The crystallinity of the basalt as well as the solution concentrations (i.e., pH) are varied in order to characterize a number of different possible surface conditions.

While synthesizing our basalt to address this central question, we found that chromite appears to be an important phase in some basalt with Martian compositions. We decided it would be beneficial for our study of Cr mobility to obtain a better

understanding of chromite dissolution. Accordingly, weathering experiments were also performed on two chromites at a variety of pH's and water-rock ratios.

Chapter 2

Materials and Methods

2.1 Basalt - Experimental Methods

2.1.1 Basalt Synthesis

The basaltic analog composition used in this study is based on an average Cl- and S-free Pathfinder soil (PFS), originally derived by *Tosca et al.* [2004] with the addition of Ni, Zn, and Cr (Table 2). The major element composition was chosen to approximate an average Martian crust composition, while the trace element concentrations were chosen also being mindful of instrumental detection limits and the stability of related minerals. This composition was selected prior to the landing of the MER rovers and so the average composition of the Martian soils and average Martian crust is now much better understood (e.g., *Taylor and McLennan*, 2009). However, the average Pathfinder soil composition is close enough to our current understanding of Martian crustal composition that the benefit from previous experimental experience with this composition [*Tosca et al.*, 2004] was felt to outweigh any slight compositional differences.

Two batches of synthetic basalt were prepared utilizing a mixture of powdered oxide and silicate components designed to match the desired bulk chemical composition. The components are each accurately weighed and placed into a mechanized agate mortar and pestle where they are ground and mixed together with ethanol for a period of 4 hours. After the mixture is thoroughly homogenized, it is dried and loaded into 1-inch, 2.5

Table 2. Synthetic Analog Bulk Composition

Oxides, wt %	PFS Target[a]	PFS Average[b]	Irvine[c]	Island Arc[d]
SiO_2	48.42	48.78	48.40	50.23
TiO_2	1.17	1.18	1.09	1.02
Al_2O_3	10.29	10.77	8.54	16.71
FeO_T	19.10	18.05	19.77	8.66
Cr_2O_3	0.10	0.09	0.21	0.11
MnO	0.49	0.50	0.37	0.17
MgO	8.00	8.19	10.95	9.21
CaO	7.15	6.89	6.21	11.17
Na_2O	3.55	3.56	2.76	2.42
K_2O	0.65	0.57	0.70	0.21
P_2O5	1.18	1.32	1.00	0.10
Total	100.00	100.00	100.00	100.00
Ni*	1000.00	740.00	289	152.00
Zn*	1000.00	690.00	230	68.00

[a] Composition taken from *Tosca et al.* [2004] with the addition of Ni, Zn, and Cr.
[b] Average of 10 analyses, normalized to 100%
[c] Composition recalculated to exclude volatiles, normalized to 100%
[d] New Britian Island Arc Basalt, recalculated to exclude volatiles, normalized to 100%
* Element concentration in ppm

diameter $Au_{80}Pd_{20}$ capsules. The capsule, which is sealed at one end, is placed into silica glass tubing.

One major challenge we encountered while synthesizing our basalts was the persistence of chromite at the calculated liquidus (see Appendix A). In order to decrease, and hopefully eliminate, the amount of chomite in our basalts we lowered the oxygen fugacity using a wustite-magnetite redox buffer. The wustite-magnetite buffer is made with a mixture of Fe^o and Fe_2O_3 components that are ground until completely homogenized. The mix is placed into silver foil, dried and sealed in silica tubing under vacuum. The buffer mix is placed into a furnace and allowed to react for one week. After this time the mix is removed from the silver foil and placed into platinum capsules. The capsule containing the buffer is placed above the $Au_{80}Pd_{20}$ capsule in the silica glass tube, which is then sealed at one end. The open end of the tubing is drawn out into a thin capillary using an oxy-acetylene torch and a piece of Fe metal is placed on top (Figure 3). The silica tube is then placed under vacuum while it is dried for a period of 40 minutes. The silica tube assembly was chosen such that the basalt sample is at approximately 800 °C while the Fe metal is at 600 °C, which prevents any volatiles that may be released from oxidizing the sample. While still under vacuum, the capillary is melted and separated using the torch to create a sealed silica assembly.

Platinum wire is used to attach the silica tube assembly to a pair of electrodes, which is slowly lowered into a vertical $Pt_{90}Rh_{10}$-wound furnace where it is raised above its liquidus (Figure 3). To quench the sample a current is sent down the electrodes in the furnace to melt the platinum wire. The silica tube is released into a beaker of cold water forming basaltic glass. The basalt that was allowed to crystallize is quenched after

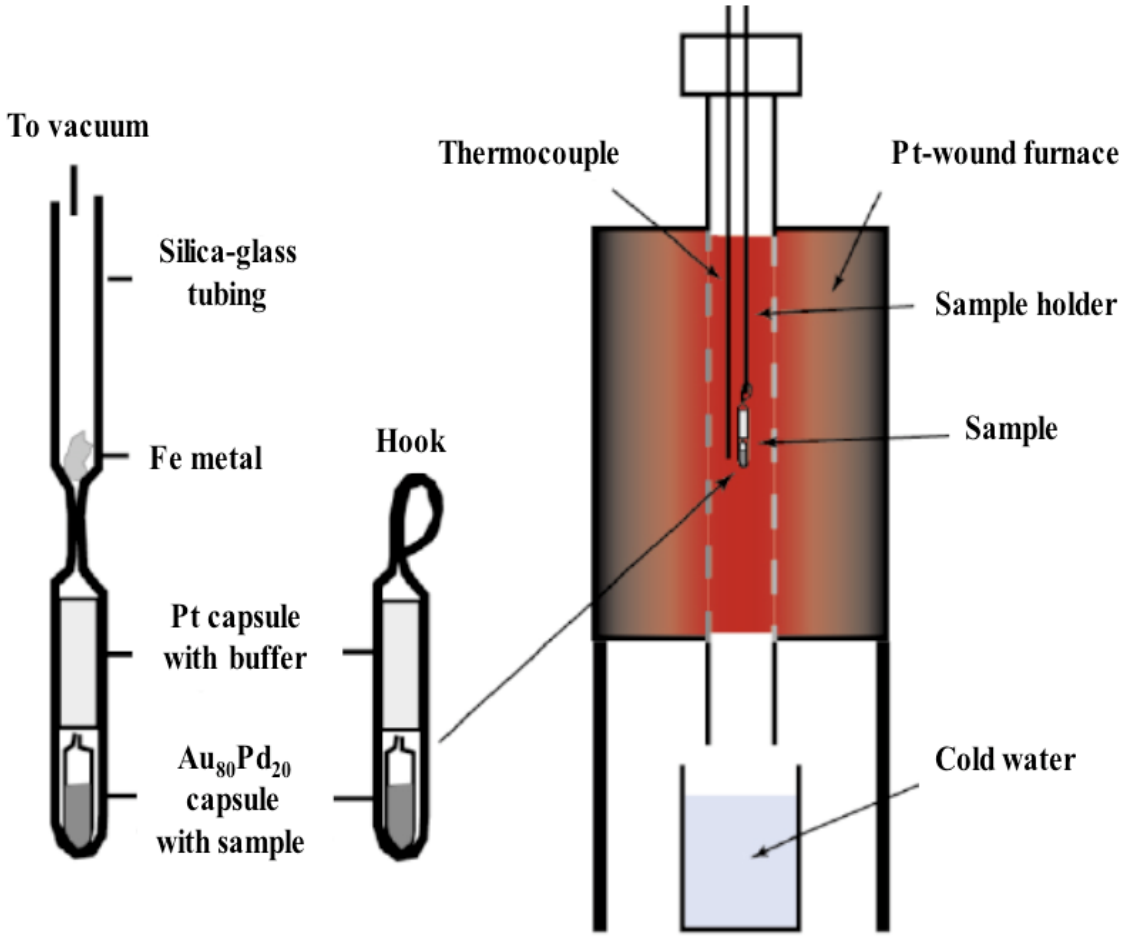

Figure 3. Schematic of basalt synthesis procedures

following a gradual step-by-step cooling path in which dwelling is permitted at different crystallization temperatures. We refer to these samples as crystalline basalt. Due to the temperature gradients within the furnace, only a small amount of basalt (approximately 300 mg) can be synthesized at one time.

A few extra steps were taken to synthesize both our glass and crystalline basalts. First, *Tosca et al.* [2004] had reported approximately 7 relative percent Fe° loss to the

$Au_{80}Pd_{20}$ walls while performing similar experiments. To compensate for the loss of Fe to the walls, an excess of Fe° was added to the oxide mixtures. Experimental observations also showed a loss of both Zn and Ni to the walls of the $Au_{80}Pd_{20}$ tubing (see Appendix A). This complication was overcome by adding extra NiO and ZnO to the oxide mixture. Lastly, the kinetics of plagioclase formation under laboratory conditions is very slow. *Tosca et al.* [2004] had success by nucleating plagioclase using a method that involved sub-solidus equilibration of the oxide mixture prior to synthesis. Pre-reacting the mix at 900 °C for a period of ten days is believed to react Al, Ca and Si grains that form a plagioclase seed that is stable up to higher temperatures [*Tosca et al.*, 2004]. Only one of our attempts to form plagioclase using this method was successful. Therefore, only one experiment was performed on the basalt that had crystallized plagioclase (crystalline basalt experiment F) while the other experiments were performed on crystalline basalt that did not contain plagioclase (experiments A-E).

2.1.2 Aqueous Batch Experiments

The resulting basalt was removed from the platinum capsule and crushed with a metal mortar and pestle. The samples were sieved to limit the particle size between 63 and 710 µm. The products were then ultrasonically rinsed in acetone to remove ultrafine particles and dried overnight. The dried basalt was divided up between five Teflon® beakers that contained varying concentrations of sulfuric and hydrochloric acids in order to achieve a water-to-rock ratio of 10. Acid mixture concentrations ranged from a 1 M

H_2SO_4/0.25 M HCl mix to 100 μM H_2SO_4/25 μM HCl, each with a S:Cl molar ratio of 4 (Table 3) which is comparable to typical Martian soils. Fluid samples were taken throughout the course of the 14 day alteration period. The samples were then diluted with 4% HNO_3, filtered using 0.20 μm nylon syringe filters and refrigerated before further analysis. The volume of sample removed during each sampling was such that upon conclusion of the experiments less than 4% of the total starting fluid had been removed.

At the end of the 14 days, the beakers were placed into an oven where remaining fluids were evaporated below 60°C to avoid volatilization of HCl [*Banin et al.*, 1997]. After two days the beakers were removed from the oven and the remaining solids were rinsed in a vacuum filter with anhydrous ethanol using a 0.45μm nitrocellulose filter. The solids were allowed to air dry until all the ethanol had been evaporated. No attempts were made to control the relative humidity of these experiments.

Table 3. Acid mixtures used in alteration experiments

Acid Mixture	H_2SO_4 (mol/L)	HCl (mol/L)
A	1.0×10^{0}	2.5×10^{-1}
B, F	1.0×10^{-1}	2.5×10^{-2}
C	1.0×10^{-2}	2.5×10^{-3}
D	1.0×10^{-3}	2.5×10^{-4}
E	1.0×10^{-4}	2.5×10^{-5}

2.2 Chromite – Experimental Methods

2.2.1 Chromite Composition and Aqueous Batch Experiments

The addition of chromium to our Martian basalt composition stabilized chromite at 1248° C, a temperature that had been the calculated liquidus of the PFS chromium-free basalt composition utilized in the previous study [*Tosca et al.*, 2004]. Chromite continued to persist over a variety of conditions and it became clear that this is an important phase in basalt compositions that were similar to those found on the Martian surface. To increase our understanding of the processes that aid in chromite dissolution, we performed a series of weathering experiments on two different chromites.

The chromites used in this study were natural samples. The chromite referred to as C6 is from the Stillwater Complex in Montana. The second was a research grade chromite obtained from Ward's Scientific (49-5936) and will be referred to as CW. The compositions of both samples can be found in Table 4.

The samples were crushed and then chromite grains were hand picked under a stereomicroscope in an attempt to exclude small amounts of other phases. The samples were then sieved to limit the particle size between 63 and 710 µm and checked again for unwanted phases. They were then ultrasonically rinsed in acetone and dried overnight.

The two sulfuric and hydrochloric acid mixtures utilized in these experiments had the same concentrations as A and C seen in Table 3. Experiments were performed with fluid-to-chromite ratios of 10 and 100. A summary of the experiments performed can be seen in Table 5. All fluid-chromite mixtures were enclosed in Teflon® beakers and allowed to react at room temperature for a period of about 7 weeks. During that time fluid samples were taken and diluted with 4% HNO_3. As with the basalt experiments, fluid

Oxides, wt %	C6	CW
MgO	11.52	12.77
Al_2O_3	18.96	8.48
Cr_2O_3	43.73	58.73
MnO	0.17	0.17
FeO	24.86	19.49
TiO_2	0.56	0.18
ZnO	0.07	0.07
NiO	0.13	0.11
Total	100.00	100.00

Table 4. Composition of chromites used in alteration experiments. Compositions are an average of 10 analyses normalized to 100%.

C6		CW	
pH	water:rock	pH	water:rock
0	10:1	0	10:1
2	100:1	2	100:1
0	100:1	0	100:1
2	10:1	2	10:1

Table 5. Summary of chromite experiments performed in this study.

samples were filtered using 0.20 μm nylon syringe filters and refrigerated before further analysis. The volume of sample removed during each sampling was such that upon conclusion of the experiments less than 4% of the total starting fluid had been removed. At the end of the experiments the remaining fluids were completely evaporated in all of the experiments with a starting pH of 2. The solutions in the experiments with a starting pH of 0 never fully evaporated.

2.3 Analytical Methods

In order to determine the accuracy of the synthesized basalt composition to the target composition, all basaltic materials were chemically analyzed before weathering. As the compositions of the chromite samples were unknown they also had to be analyzed before acid alteration. Chemical compositions were determined with a Cameca Camebax Micro electron microprobe equipped with four wavelength-dispersive spectrometers and a Kevex Analyst 8000 energy-dispersive detector. An accelerating voltage of 20 kV was used during all analysis. A beam current of 20 nA was used to analyze major elements and the trace elements were analyzed using a beam current of 30 nA. When analyzing Na-bearing material the largest raster size possible was used to reduce the loss of Na to volatilization.

X-ray diffraction (XRD) was utilized to determine the initial mineralogy of the crystalline basalt and to verify the purity of the chromites. All XRD analyses were performed using a Scintag PAD X diffractometer with $CuK\alpha_1$ radiation at 40 kV and 25

mA. All data were collected between 10 and 70 degrees 2θ, with a scan step size of 0.02 degrees, except for the chromite samples, which were collected between 15 and 90 degrees 2θ. Diffraction patterns were matched to those in a Powder Diffraction File (PDF), a phase identification database, using the Crystallographica Search-Match© program.

All samples taken throughout the alteration periods were analyzed using a Beckman Spectraspan SSVB Direct Current Plasma Atomic Emission Spectrometer (DCP-AES) to determine the concentrations of dissolved cations in solution. The pH of the solutions was calculated by entering complete solution analysis and total S and Cl concentrations into the geochemical modeling program Visual MINTEQ [Gustafsson, 2004]. This program is able to calculate the pH of solutions by charge balance from speciation calculations. We were not able to measure pH directly in the basalt solution as electrolyte solutions used with various pH electrodes might have contaminated the samples. However, elements commonly used in electrolyte solutions were not the elements of interest in our chromite experiments. As a result, solution pH of the chromite experiments was also measured at the conclusion of their alteration.

At the end of the alteration process, all remaining fluids were evaporated and residual materials were analyzed with the XRD (as described above). To detect the presence of minor phases and poorly crystalline material all samples (excluding the chromite experiments with a starting pH of 0) were also examined with a LEO Gemini 1550 SFEG scanning electron microscope (SEM). All analyses were performed using an accelerating voltage of 15 kV. The SEM is also equipped with an EDAX energy dispersive X-ray spectrometer, which is capable of identifying the elemental components

of individual particles. However, in order to obtain a somewhat quantitative chemical formula, the surface of the particle has to have a relatively flat topography. In this study most analyses were performed on samples with variable surface angles but a stoichiometric comparison between elements in the spectra can aid in identifying mineral phases.

Chapter 3

Results

3.1 Basalt and Glass Synthesis - Results

The resulting synthesized basalt composition, seen in Table 2, was determined with an electron microprobe. The program *MELTS* [*Ghiorso and Sack*, 1995] was used to determine equilibrium modal mineralogy of crystalline basalts. Phase equilibria were calculated using the bulk glass composition as the starting material. Other data entered into the program included crystallization temperatures, a fixed oxygen fugacity and a pressure of 1 bar. The calculated mineralogy was compared to the mineralogy in our crystalline basalt in order to determine that the crystallized basalt was close to equilibration.

The electron microprobe was also used to verify that the synthesized glasses were homogeneous. A cross section was taken of a quenched sample so that a number of point analyses could be performed. It was found that there was very little variation in the composition of the glass from one analysis to the next including analysis that were taken right next to the capsule wall. This indicates that the glass was completely homogeneous and that the Fe loss to the capsule walls was not just an edge effect. It was concluded that the glass was close to if not completely homogeneous.

The target oxygen fugacity was in the range of the wustite-magnetite buffer. The actual oxygen fugacity conditions of the crystallized basalt was calculated using the

program QUILF [*Andersen et al.*, 1993]. The fugacity was calculated to be one log unit above the FMQ buffer for the crystalline basalt without plagioclase and 0.1 log units below the FMQ buffer for the crystalline basalt with plagioclase. Even though a wustite-magnetite buffering capsule was utilized during the synthesis of these basalts the resulting oxygen fugacities are not as reduced as the desired oxygen fugacity. This may be due to the formation of magnetite from wustite during oxidation within the buffer capsule. The presence of the magnetite may have formed a barrier on top of the remaining material, which would prevent the oxidation of any additional wustite below this barrier, hence, stopping any further reduction of the basalt. The mineral formulas for olivine, pyroxene and the Fe-Ti oxides were also calculated using the QUILF program (see Table 6).

3.2 Basalt Alteration Experiments - Results and Interpretations

Here we present the results for the basaltic glass and the crystalline basalt. Each results section will be followed by a brief discussion and interpretation of the data. Full solution analyses for each experiment can be found in Appendix B and a summary of secondary phases found in the basalt experiments can be found in Table 7.

Table 6. Modal abundances for both crystalline basalts determined by least squares analysis of electron microprobe data.

PFS Basalt (no plag)		PFS Basalt (plag-bearing)	
Olivine ($Fo_{62}Fa_{38}$)	23.40%	Olivine ($Fo_{57}Fa_{43}$)	24.90%
High-Ca pyroxene ($Wo_{38}En_{43}Fs_{19}$)	9.80%	High-Ca pyroxene ($Wo_{37}En_{36}Fs_{27}$)	24.50%
Feldspar ---	0.0%	Feldspar ($Ab_{66}An_{32}Or_{2}$)	31.70%
Fe-Ti oxides ($Mt_{60}Usp_{40}$)	0.50%	Fe-Ti oxides ($Mt_{24}Usp_{76}$)	4.50%
Chromite	1.70%	Chromite	0.30%
Interstitial glass	64.60%	Interstitial glass	14.30%

3.2.1 Basaltic Glass - Solution Chemistry and Secondary Phases

Within the first 48 hours the basaltic glass that had been reacted with solution A appeared as a while gel-like material. The glass in this experiment had almost completely dissolved, releasing a very large number of ions into solution (Figure B1) that precipitated when the solution became oversaturated. Similar to results found in previous studies [*Tosca et al.*, 2004], the most abundant elements in solution in experiment A are Fe, Mg, Al and Na followed by Si and Ca (Figure B1). The presence of Si and Ca enriched residual solids (see below) supports the idea that these two elements were more abundant in solution but were quickly precipitated out when saturation states of a Si-bearing phase and a Ca-bearing phase were exceeded.

The Na/Mg ratios shown in Figure 4a indicate that in the experiments with the lowest pH solutions (A, B and C) the glass dissolves in near-stoichiometric proportions with respect to major elements. Divalent and univalent network-modifying elements are stoichiometric in solution in experiment A, suggesting they are leached by similar methods (Figure 4b). In contrast, experiments D and E dissolved in a non-stoichiometric manner that appears to have preferentially released univalent elements (see Discussion section below). Also in experiments D and E, the concentration of Fe in solution was comparatively low, as was the Fe/Mg ratio during the last sampling of these experiments (Figure 5a), suggesting iron oxidation in solution.

The trace elements Ni, Zn and Cr were also released in stoichiometric proportions in the lower pH solutions. For example, Cr and Al, two trivalent elements, were released in close to stoichiometric proportions in experiments A and B (Figure 4a). Ni also appears to have dissolved in close to stoichiometric proportions with respect to other divalent elements (Figure 4a). At more basic pH's however, dissolution became

Table 7. Secondary products identified in the PFS basalt experiments.

	PFS Glass					PFS Basalt					PFS Basalt with Plag
	A	B	C	D	E	A	B	C	D	E	F
Amorphous SiO_2 (from solution)	E	E	E	E	-	E	E	E	E	-	E
Amorphous SiO_2 (leached layers)	-	E	E	-	-	-	E	-	-	-	-
Alunogen ($Al_2(SO_4)_3 \cdot 17H_2O$)	X, E	X, E	E	-	-	-	-	-	-	-	-
Anhydrite ($CaSO_4$)	X, E	X	-	-	-	-	-	-	-	-	-
Gypsum ($CaSO_4 \cdot 2H_2O$)	X, E	X, E	E	E		-	E	E	E	-	X, E
Fe oxide	-	-	-	E	E	-	-	-	E	E	-
$FeSO_4 \cdot nH_2O$	-	-	-	-	-	E	-	-	-	-	-
Hexahydrite ($MgSO_4 \cdot 6H_2O$)	X	X	-	-	-	-	X	-	-	-	X
Kieserite ($MgSO_4 \cdot H_2O$)	-	-	-	-	-	X, E	-	-	-	-	-
$MgSO_4 \cdot nH2O$	E	-	-	-	-	E	E	-	-	-	E
Melanterite ($(Fe,Mg)SO_4 \cdot 7H_2O$)	X, E	X, E	E	-	-	E	X, E	-	-	-	X, E
Tamarugite ($NaAl(SO_4)_2 \cdot 6H_2O$)	X	E	-	-	-	-	-	-	-	-	-

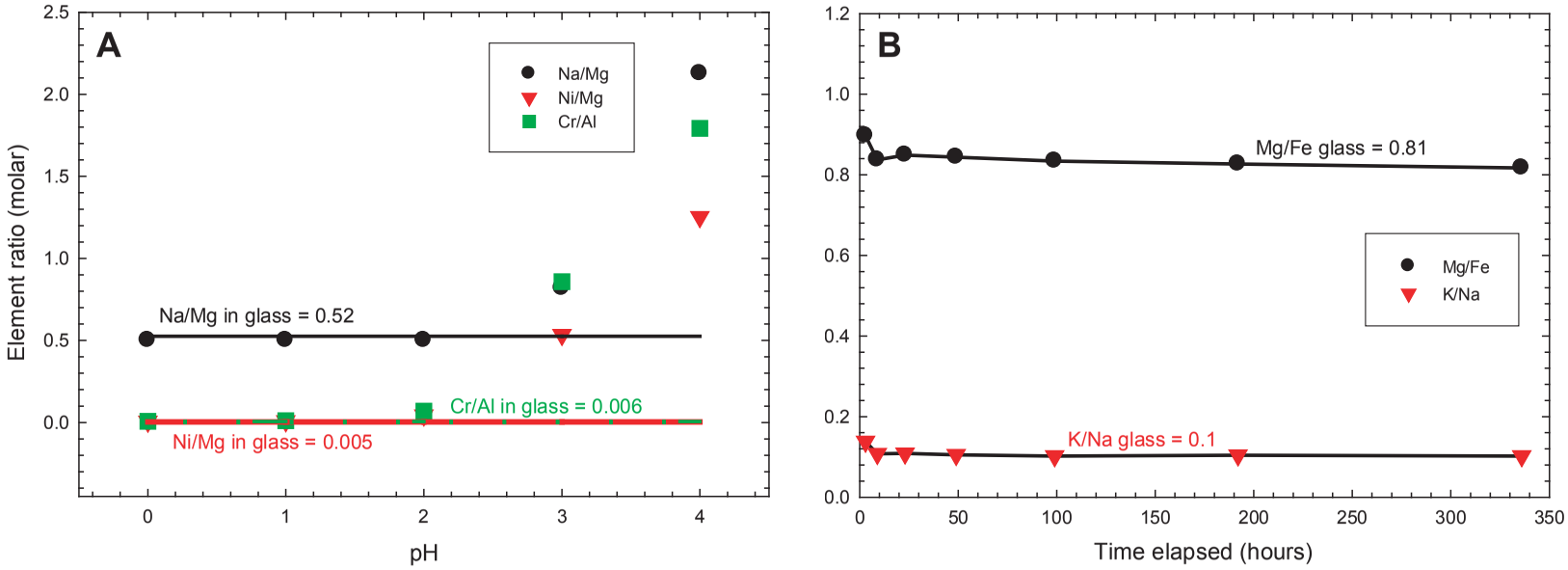

Figure 4. (a) Element to element ratios versus pH in PFS glass solutions at 336 hours. All elements appear to have dissolved stoichiometrically in low pH fluids (0-2), while at higher pHs they dissolve in non-stoiciometric proportions. (b) Mg/Fe and K/Na ratios versus time in PFS glass, solution A. These ratios show that divalent and univalent network modifying elements are stoichiometric in solution, suggesting they are leached by similar mechanisms.

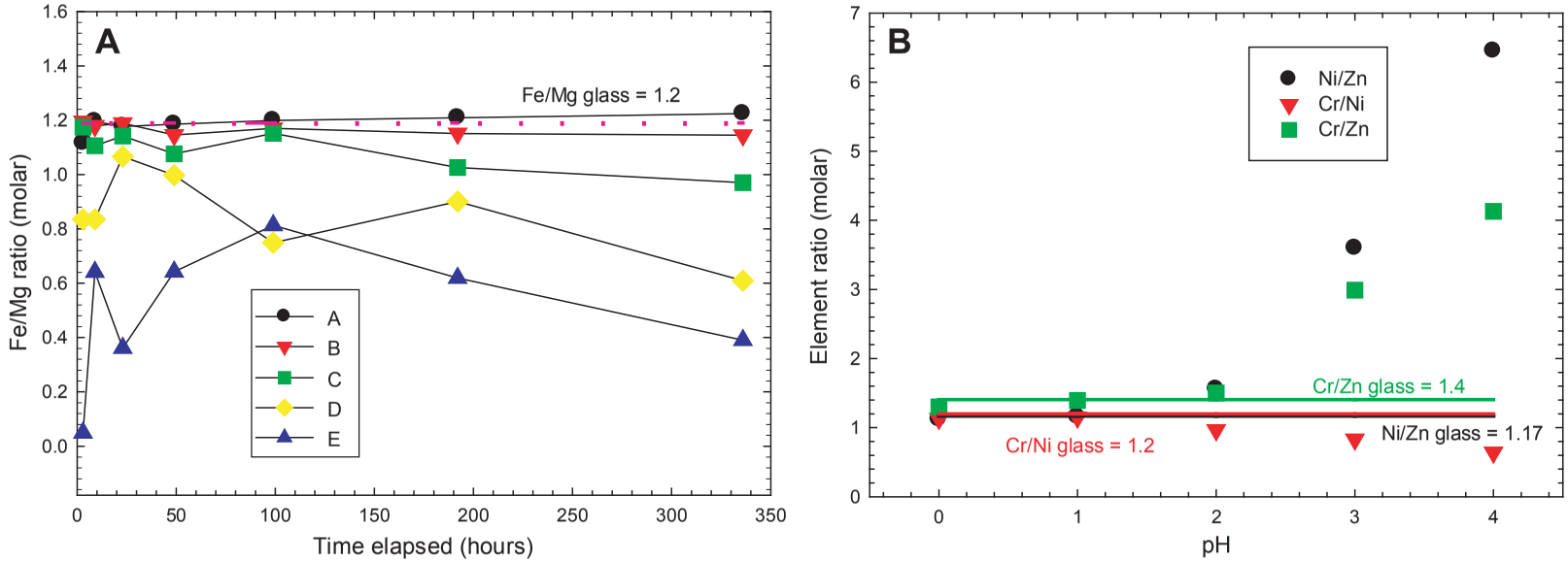

Figure 5. (a) Fe/Mg ratio versus time in PFS glass, Solutions A-E. The Fe/Mg ratio is low in experiments D and E which may indicate Fe oxidation. (b) Trace element to element ratios versus pH in PFS glass at 336 hours. The trace elements appear to have dissolved in the order Ni>Cr>Zn.

non-stoichiometric so that Ni was relatively more abundant in solution than Mg and Cr is relatively more abundant than Al. When compared to each other these trace elements appear to have been removed from the solid in the order: Ni > Cr > Zn (Figure 5b).

Figure 6 shows SEM micrographs of the basaltic glass grains for all five experiments and the abundance of secondary phases formed in each one. The residual solids found in these experiments consist of amorphous silica that has been precipitated from solution, silica rich layers from leaching of the glass surface, and secondary evaporite and oxide minerals (Table 7).

The residual solid found in experiment A consists mainly of amorphous silica with only a very small amount of the original basaltic glass grains remaining. The amount of amorphous silica that has been precipitated in each experiment decreases as the pH increases. In experiments B and C leached layers were found covering most of the basaltic glass grains. These layers were found to be rich in Si and O and occasionally had detectable amounts of Al (determined by EDS). In places where these layers had been removed fresh basaltic glass remained underneath. Both the precipitated amorphous silica and the leached layers can be seen in Figure 6.

The hydration states of the following minerals must be interpreted carefully as no attempts were made to control the relative humidity of these experiments. Al-sulfate phases were identified in experiments A-C upon evaporation. XRD analysis identified tamarugite ($NaAl(SO_4)_2 \cdot 6H_2O$) and alunogen ($Al_2(SO_4)_3 \cdot 17H_2O$) in experiments A (Figure 7). SEM/EDS analysis identified tamarugite in experiment B and verified the presence of alunogen in experiments A and B. A very similar Al phase, believed to be alunogen, was also identified by SEM/EDS in experiment C. The Ca sulfate phases

gypsum ($CaSO_4 \cdot 2H_2O$) and anhydrite ($CaSO_4$) were identified by XRD and SEM/EDS in experiment A. Gypsum was also found to be present in experiment B by both XRD and SEM/EDS analysis, while anhydrite was only identified by XRD in this experiment. Additionally, a small abundance of gypsum was found to be present by SEM/EDS in experiments C and D.

Hexahydrite ($MgSO_4 \cdot 6H_2O$) was identified in experiment A with XRD (Figure 7) and a Mg sulfate with unknown water content was found by SEM/EDS analysis. Mg was also present in Mg-bearing melanterite ($(Fe,Mg)SO_4 \cdot 7H_2O$) that was found by XRD and SEM/EDS in experiments A and B and by SEM/EDS in experiment C. Fe was also identified in oxide phases by SEM/EDS in Experiments D and E only, which supports the suggestion that these two experiments experienced oxidation in solution (see above).

3.2.2 Basaltic Glass - Interpretation and Discussion

When attempting to constrain processes that lead to the mobility of cations in these experiments, it is essential to understand the structure of glass. According to *Zachariasen* [1932], glass is made up of glass-forming cations, (such as Si and Al) that are surrounded by corner sharing oxygen tetrahedra. These cations (also known as network-forming elements), together with oxygen atoms, are responsible for the framework of glass. The atoms located in the structural cavities of this framework are referred to as network modifiers. When modifying elements (such as K and Na) are

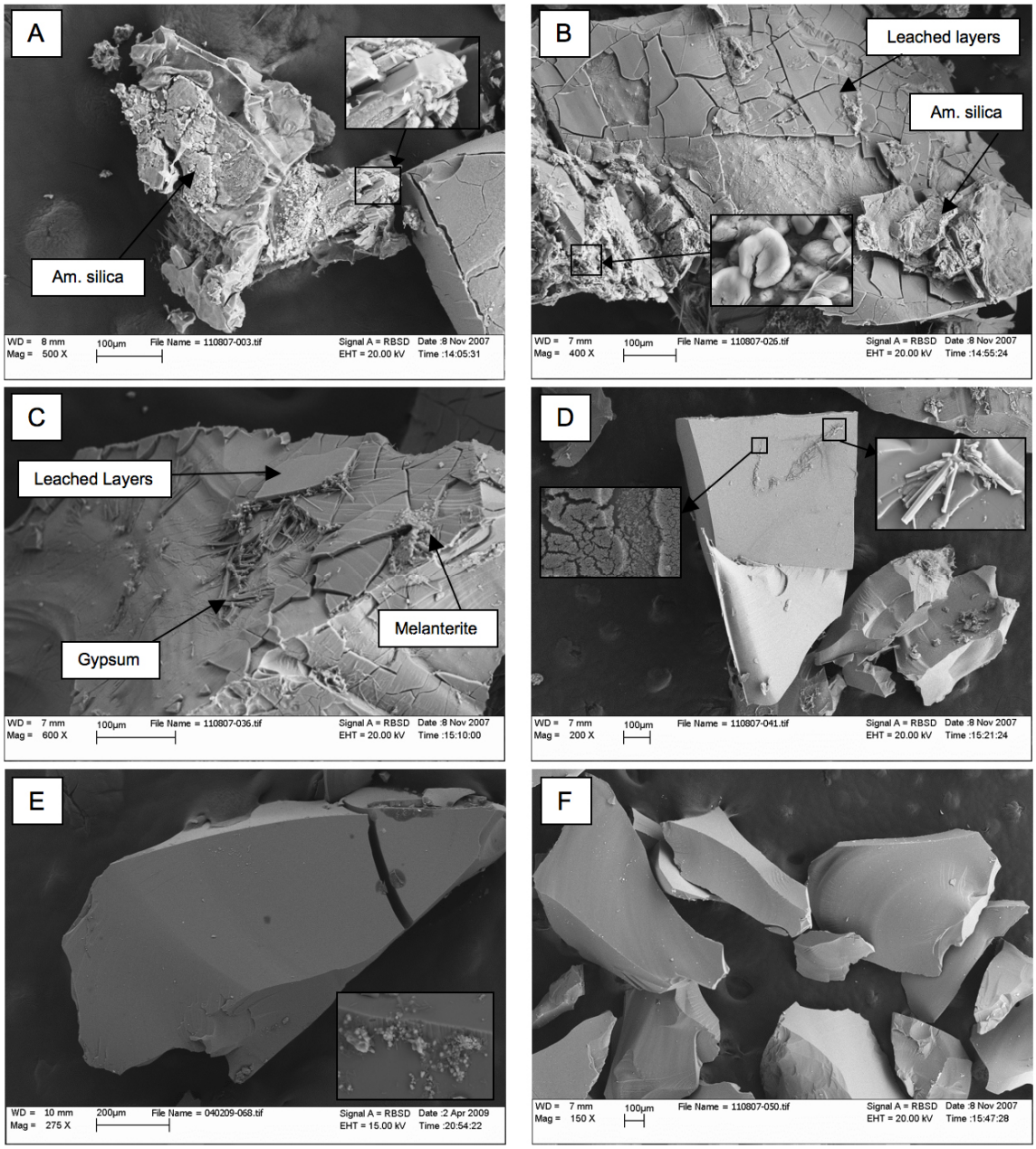

Figure 6. Scanning electron micrographs of PFS glass: (a) reacted with solution A (insert: gypsum), (b) reacted with solution B (inset: melanterite), (c) reacted with solution C, (d) reacted with solution D (left inset: iron oxides, right inset: gypsum), (e) reacted with solution E (inset: Fe oxides), and (f) unreacted basalt.

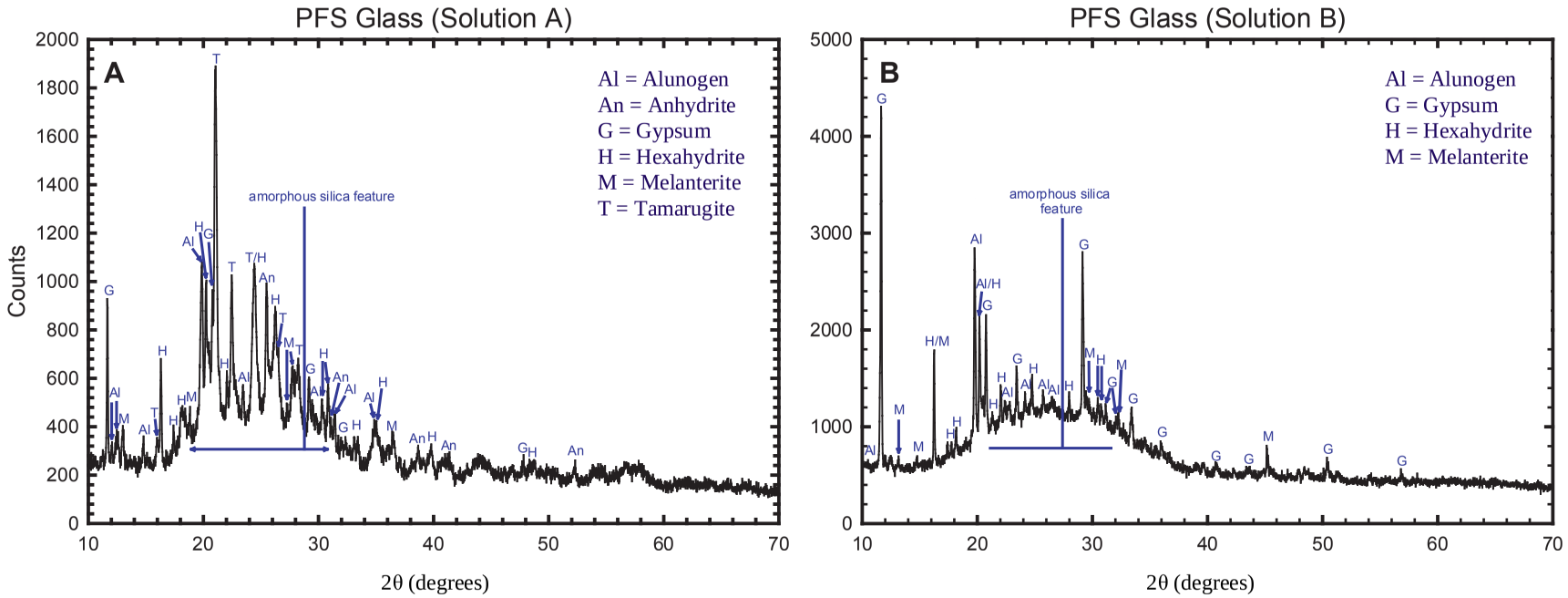

Figure 7. X-ray diffractograms for the only two samples that contained identifiable secondary phases in the PFS glass experiments. (a) PFS glass, Solution A, (b) PFS glass, Solution B.

incorporated into the structure they may cause bond breakage between the glass-forming cations and the oxygen atoms, which results in depolmerization of the overall structure [*Bouska*, 1993; *Casey and Bunker*, 1990; *Zachariasen*, 1932]. Accordingly, when the abundance of network-modifying elements is increased there is a decrease in bridging oxygens, which leads to an increase in structural disordering [*Bouska*, 1993].

As network-modifying elements are bound less tightly to the surrounding oxygen atoms than network-forming elements [*Zachariasen*, 1932], the rate at which an element will be released into solution will depend on its coordination within the glass structure (network-modifying vs. network-forming). For example, the network-modifying element Na will be released into solution preferentially when compared to Si, a network-forming element due to the stronger bonds within the network-forming sites. If one element can occupy both sites then the rate of release will depend on which site has the majority of the ions. This is believed to be the reason for the silica-enriched layers we find in experiments B and C. Due to their weaker bonding to the surrounding oxygen atoms, the network-modifying elements are preferentially removed from the surface of the basalt, leaving behind a layer that contains mainly networking forming elements such as Si.

Another important aspect to understanding the release of cations from glass is the valence of the element of interest. During the initial stage of glass dissolution the rate of element release is proportional to the elements oxidation state [*Bouska*, 1993; *Oelkers and Gislason*, 2001; *Zachariasen*, 1932]. This is consistent with what we see in our experiments and is illustrated with the Na/Mg ratio in solution (Figure 4). As previously mentioned, in experiments C and D it appears that univalent cations (Na in this case) are being released preferentially to divalent cations (Mg) within the network-modifying site.

In the case of Ni, Cr, and Zn mobility, we must first discuss their coordination and valency within the structure of glass. According to Roeder and Reynolds (1991), a Cr-bearing basaltic melt at an oxygen fugacity equivalent to the FMQ buffer contains 70% of its total Cr content as Cr^{3+} and 30% as Cr^{2+}. However, the Cr^{2+} within the melt is not retained in glass due to an electron exchange reaction with Fe^{3+} that occurs on quenching [*Berry et al*., 2006]. Consequently, Cr is believed to occur exclusively as Cr^{3+} in our Fe-bearing basaltic glass. Due to its high field stabilization energy, trivalent chromium occurs only in octahedral coordination in glass and most crystalline compounds [*Calas et al.*, 2006; *Murck and Campbell*, 1986].

In contrast, Ni is always found to be divalent in the oxygen fugacity range relevant to this study. Its coordination within the structure of glass, however, is a little more complex. Ni has been found to exist in 4- and 5- coordination ($^{[4]}$Ni and $^{[5]}$Ni, respectively) in oxide glasses, the proportion of which is dependent on the composition of the glass [*Calas et al*., 2002; *Cormier et al*., 2001; *Galoisy and Calas*, 1991, 1992, 1993a, 1993b; *Galoisy et al*., 2000]. $^{[4]}$Ni is predominant in potassic glasses while $^{[5]}$Ni prevails in glasses that contain higher field strength cations such as Na, Ca, and Mg [*Galoisy and Calas*, 1992, 1993a, 1993b]. As our glasses contain abundant amounts of these higher field strength cations and very little K it is assumed $^{[5]}$Ni is the predominant coordination. Unlike $^{[4]}$Ni, $^{[5]}$Ni does not appear to have a direct connection with the silicate framework [*Calas et al*., 2002].

Lastly, Zn is also found to be divalent in our oxygen fugacity range. There is some disagreement as to what coordination this trace element takes in the structure of glass. Some argue that Zn can be found in tetrahedral ($^{[4]}$Zn) or octahedral ($^{[6]}$Zn)

coordination, with a preference for tetrahedral coordination [*Calas et al*., 2002; *Le Grand et al.,* 2000]. In this situation, it is believed that the $^{[4]}Zn/^{[6]}Zn$ ratio increases as the Zn/Na ratio decreases due to the Na ions ability to compensate the charge deficit of the ZnO_4 tetrahedra [*Calas et al.*, 2002; *Le Grand et al.,* 2000]. Others have argued that Zn is always found in four-fold coordination no matter the composition of the glass [*Galoisy et al*., 2000; *Cormier et al.,* 2001]. As there is an abundant amount of Na in our glass we believe it is most likely that Zn is dominantly tetrahedrally coordinated.

As mentioned previously, both major and trace elements appear to be released from the glass stoichiometrically in the experiments with the lowest pH solutions. In higher pH solutions Cr is released preferentially to Al, which can be explained by aluminum's ability to fill in for silica in the framework of glass. Also, in experiments D and E, Ni is being released into solution preferentially to Mg although they are both considered network-modifying elements. This may be due to the precipitation of Mg phases; even though none were found in these experiments they may be present in very small quantities. As Ni and Cr occupy network-modifying sites they are preferentially released over Zn, which is within the structure of the glasses framework. The element valency may explain the order in which Ni and Cr are being released. Both of these trace elements reside in the network-modifying sites but Ni, having a lower oxidation state, gets released preferentially to Cr.

3.2.3 Crystalline Basalt - Solution Chemistry and Secondary Phases

As previously mentioned, experiments were performed on two basalts with different abundances of mineral phases (Table 6). Experiments A-E contained the synthesized basalt that did not crystallize plagioclase, while experiment F was performed on basalt that did contain plagioclase.

Similar to the results found in *Tosca et al.* [2004], Fe, Mg and Si are the elements of highest abundance in solutions A-C and F (Figures B4-B7) indicating that olivine dissolution controls the solution chemistry in these experiments. At the final sampling, the Mg/Si ratio in these four solutions was close to stoichiometric with respect to the Mg/Si ratio in olivine (Figure 8a). Solutions D and E have Mg/Si ratios that are progressively lower and appear to have dissolved with a Mg/Si ratio approaching the stoichiometric proportions of pyroxene (Mg/Si ratio in pyroxene is 0.26). Abundances of Mn and P in solution were high relative to those found in PFS glass solutions. This may be due to the small amounts of these elements that are contained in the olivine.

Solution F (plagioclase-bearing sample) has much higher abundances of Ca and Al in solution compared to solution B (plagioclase-free sample) even though these two experiments have the same starting pH. The presence of plagioclase in the basalt used in experiment F may explain the elevated concentrations of these elements in solution (see Discussion section below). As plagioclase contains essentially all of the Na and Al in the basalt we can use the concentrations of these elements in solution to evaluate the dissolution of plagioclase. The higher concentrations of Na relative to Al in solution F (Figure 8c) indicates non-stoichiometric dissolution with respect to plagioclase.

Olivine also plays a role in the presence of the trace elements Ni and Zn in solution. Figure 8a shows that in the low pH solutions Ni and Mg are being released

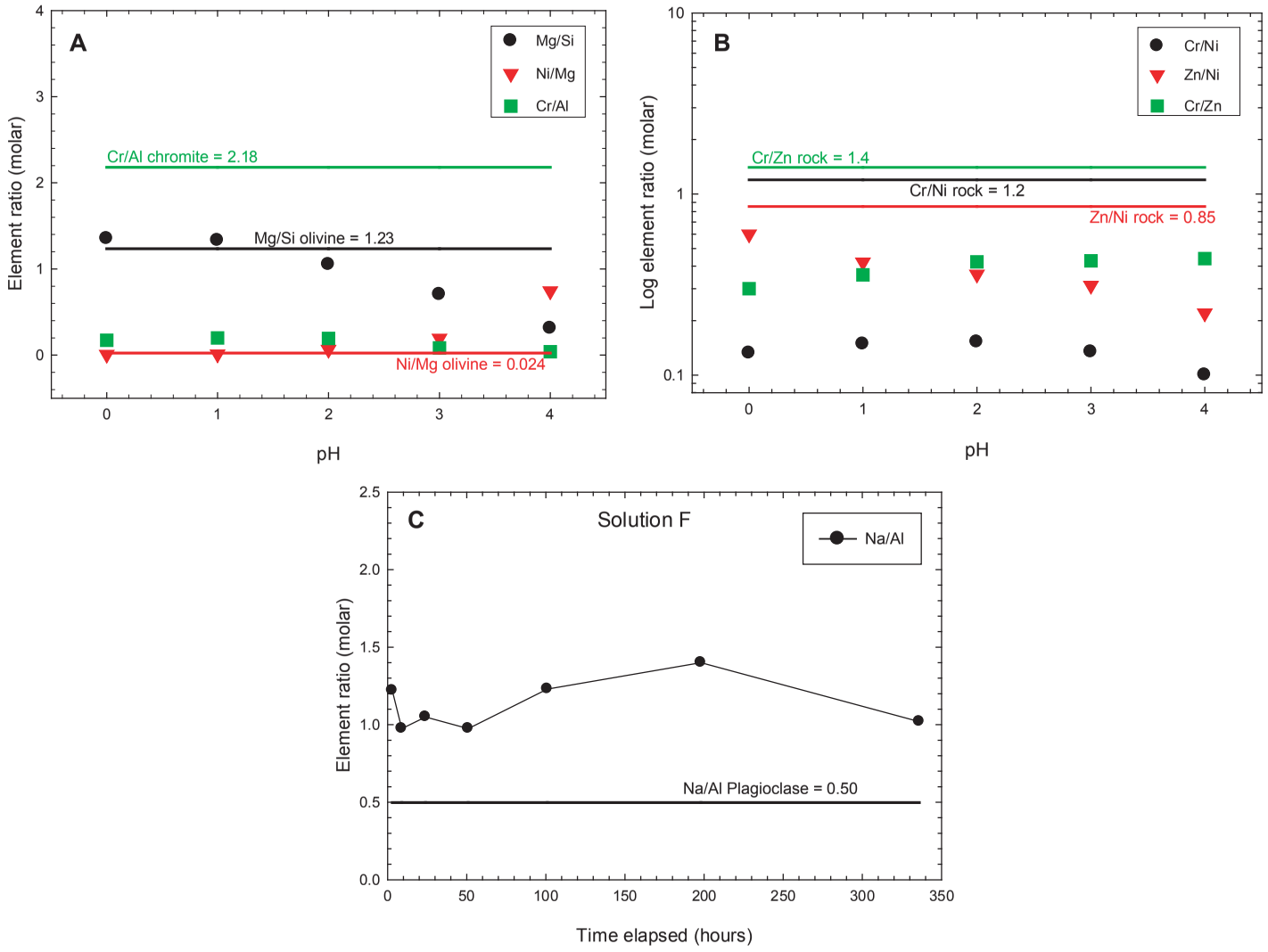

Figure 8. (a) Element to element ratios versus pH at 339 hours. (b) Trace element ratios versus pH at 339 hours. (c) Na/Al ratio versus time in PFS crystalline basalt with plagioclase.

stoichiometrically with respect to the Ni/Mg ratio in the olivine. At higher pH's however there is a small increase in the Ni/Mg ratio, indicating a slightly higher abundance of Ni relative to Mg. This is also the case for Zn relative to Mg although it is not shown in this figure. In all of the experiments performed, the Cr/Al ratio is much lower than the Cr/Al ratio in chromite, which suggests faster release of Al from the oxides or an additional phase liberating Al into these solutions (Figure 8a). Relative to each other, the trace elements Ni, Zn and Cr appear to be removed from the plagioclase-free basalt in the order: Ni > Zn > Cr. However, in the experiment that utilized the plagioclase bearing basalt, Cr is more readily leached than Zn.

As with the basaltic glass experiments, solutions A, B and F in the crystalline basalt experiments resulted in the most secondary phases, where experiments reacted with solutions C, D and E have yielded increasingly fewer phases. The decrease in secondary phases from A to E correlates to the increase in initial pH of each solution. The abundance of secondary phases can be seen in Figure 9.

Amorphous silica was identified by EDS in all experiments except for E. The largest abundances were found in experiments A, B and F while smaller amounts were detected in experiments C and D. The amorphous silica was found as precipitated aggregates in these experiments as well as layers in experiment B (Figure 9b). The crystalline basalt employed in this experiment contains a large amount of basaltic glass, which explains why these layers are similar to the ones found in the PFS glass experiments. These layers are formed by the preferential release of network-modifying elements from the glass (see above).

The presence of gypsum ($CaSO_4 \cdot 2H_2O$) was found in experiments B, C, D and F

by SEM/EDS. Gypsum was found to be much more abundant in experiment F relative to experiment B. This is most likely due to Ca concentrations in solution F, which are at least 3 times higher than those in experiment B. Gypsum was also identified by XRD in experiment F (Figure 10c).

The large amounts of Mg released into solution in these experiments produced abundant Mg sulfate minerals in experiments A, B and F. XRD analysis showed the presence of kieserite ($MgSO_4 \cdot H_2O$) in experiment A. Circular objects found in this experiment that were visible to the naked eye and identified as a Mg sulfate by the SEM/EDS are believed to be kieserite (Figure 9a). The occurrence of hexahydrite ($MgSO_4 \cdot 6H_2O$) was found by XRD analysis in experiments B and F (Figure 10) and Mg sulfates of unknown water content were also identified by SEM/EDS in these experiments. As no attempts were made to control the relative humidity of these experiments it is possible that some phases changed hydration states and no petrogenetic significance can be placed on the exact hydration states of the detected Mg-sulfate minerals.

Fe sulfates were identified in experiments A, B and F. Experiment A yielded a Fe sulfate phase when analyzed by SEM/EDS but XRD analysis did not display a secondary Fe phase. The hydration state was unable to be determined by SEM/EDS so it will be referred to as $FeSO_4 \cdot nH_2O$. In experiments B and F, melanterite ($(Fe, Mg)SO_4 \cdot 7H_2O$) was present in the XRD analyses (Figure 10) and SEM/EDS analysis confirmed this phase. The presence of Fe oxides were discovered in experiments D and E by SEM/EDS (Figure 9 d and e) although XRD analysis failed to identify any secondary materials in these experiments.

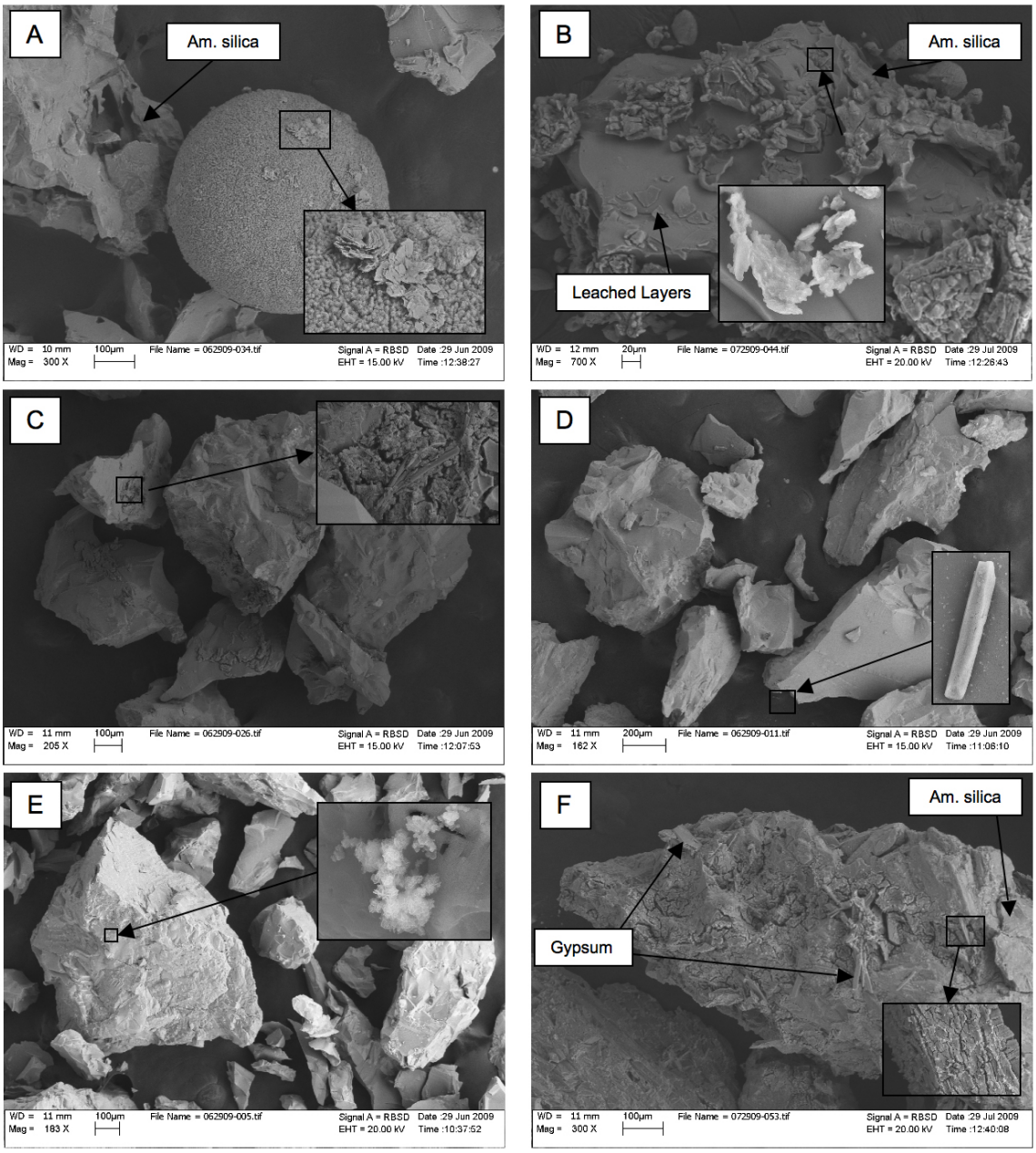

Figure 9. Scanning electron micrographs of PFS crystalline basalts: (a) reacted with solution A (inset: $FeSO_4 \bullet nH_2O$), (b) reacted with solution B (inset: melanterite), (c) reacted with solution C (inset: gypsum), (d) reacted with solution D (inset: gypsum), (e) reacted with solution E (inset: Fe oxide), and (f) crystalline basalt with plagioclase reacted with solution B (inset: bright objects are believed to be melanterite).

3.2.4 Crystalline Basalt - Interpretation and Discussion

The significant amount of protons consumed in the dissolution of these basalts most likely caused the pH to rise in the solutions with a higher initial pH (Figure B6). The more acidic solutions (A and B) have larger buffering capacities, which explain their ability to keep a nearly constant pH. Although olivine dissolution controls the solution chemistry in these experiments it is important to mention the addition of elements from other phases. In low pH solutions there is preferential release of M2 sites from pyroxene [*Burns*, 1993], which increases the concentrations of Ca (only found in M2 sites) and Mg (but to a lesser extent as it is found in both M1 and M2 sites) relative to Si [*Brantley and Chen*, 1993; *Schott and Berner*, 1985]. At higher pH, release of Mg from pyroxene is very small or negligible causing essentially congruent dissolution of Mg relative to Si [*Schott and Berner*, 1985]. The decrease of Mg dissolution from pyroxene in less acidic solutions may explain the overall progressive decrease in the Mg/Si ratio with increasing initial pH (from experiment A to E).

Similar to pyroxene, the initial stage of plagioclase dissolution consists of proton replacement for the ionically bonded cations in the near surface of the mineral, creating a leached layer [*Blum and Stillings*, 1995; *Casey et al.*, 1988; *Oelkers*, 2001; *Schott and Berner*, 1983; *Stillings and Brantley*, 1995]. The initial incongruent dissolution of plagioclase increases the concentrations of Na, Ca, K and also Al in solution. As mentioned before, these elements are present in solution at higher concentrations in the experiment that contained plagioclase, solution F, relative to solution B, which did not contain plagioclase.

The large abundance of Ni in these solutions is most likely being contributed from olivine, the phase that yields the largest concentration of Ni in the basalt. In forsteritic

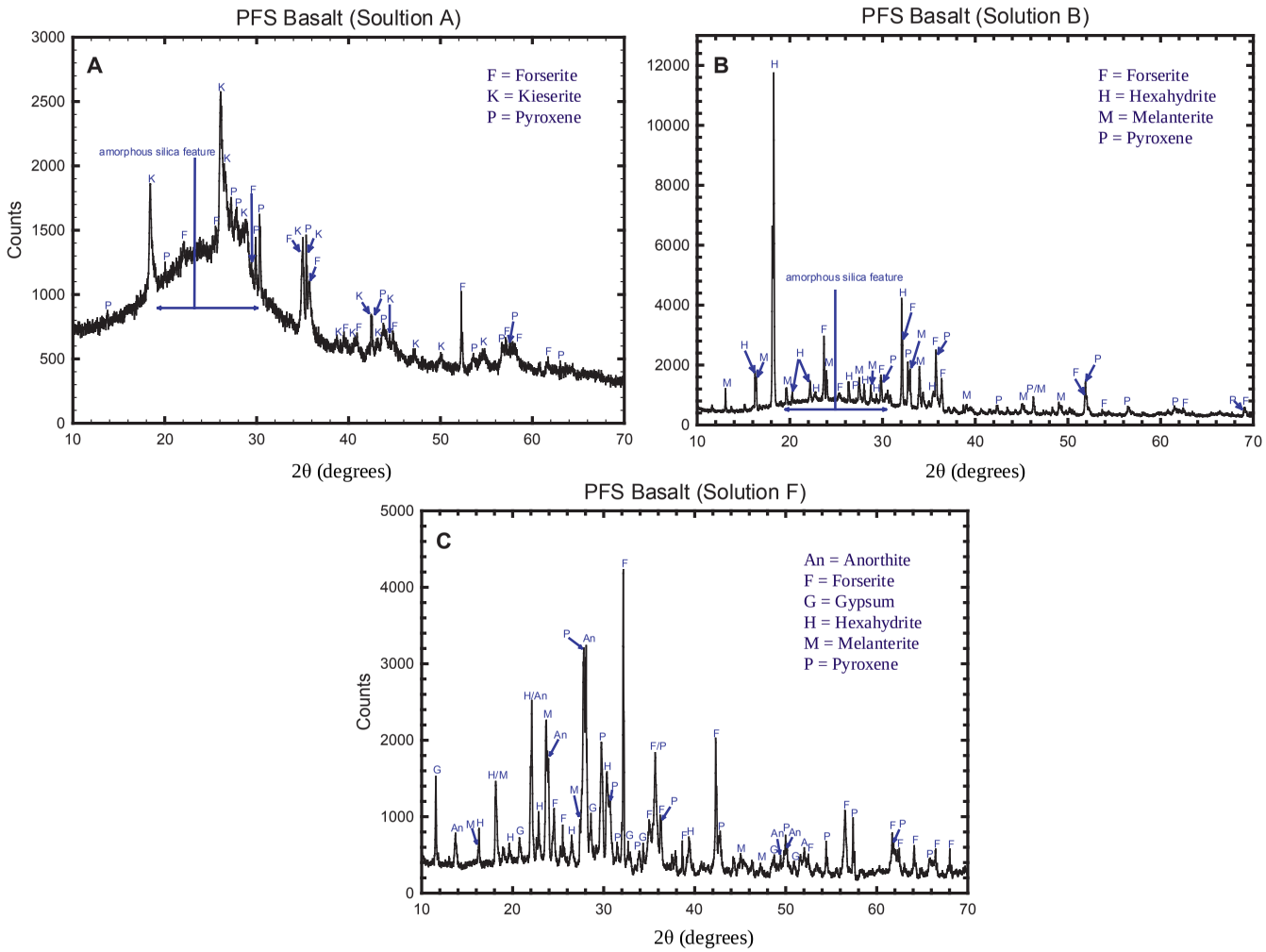

Figure 10. X-ray diffractograms for the three experiments that contained identifiable secondary phases in the crystalline basalt experiments. (a) crystalline basalt, Solution A, (b) crystalline basalt, solution B, (c) plagioclase-bearing crystalline basalt solution F.

olivine, Ni^{2+} shows a preference for the M1 site over the M2 site [*Brown*, 1982; *Burns*, 1970a, 1970b, 1973; *Dasgupta*, 1972; *Galoisy et al*., 1995]. Fe^{2+} also shows a preference for the M1 site [*Brown*, 1982] while Mg has a relative enrichment in the M2 site [*Burns*, 1973]. According to *Pokrovsky and Scott* [2000], during the initial stage of forsterite dissolution there is a slight preferential release of Fe relative to Mg, which is in agreement with the faster dissolution of fayalite relative to forsterite. Although it is unclear whether this site preference has any affect over the faster release of Fe, it may explain the preferential release of Ni, which favors the same site, relative to Mg seen in experiments D and E. Alternatively, the precipitation of Mg phases during these experiments would also increase the Ni/Mg ratio although none were detected by either XRD or SEM/EDS.

Additionally, Ni is abundant in the two spinels present in both of the synthesized basalts. This element favors the octahedral sites in spinel due to the higher crystal field stabilization energy it attains in this site [*Burns*, 1970a; *Patunc and Cabri*, 1995]. However, Ni can also occupy tetrahedral sites in the spinel structure [*Burns*, 1970a] and according to *Reynolds* [2005] will go into these tetrahedral sites in the presence of large amounts of Cr^{3+} (see below). In our crystalline basalt, Ni also occurs in pyroxene but to a lesser extent than the previously mentioned phases. In pyroxenes Ni prefers the M1 sites due to their smaller size and the larger crystal field stabilization energy it obtains [*Brown*, 1982; *Burns*, 1970a, 1970b, 1973].

Zn is also present in the olivine but is much less abundant than Ni. The olivine in the plagioclase-free basalt contains 0.15% Zn, which is about six times less than the concentration of Ni. Like Ni, Zn also prefers the smaller M1 site in olivine [*Brown*, 1982;

Burns 1970a]. In both synthesized basalts the highest concentration of Zn is found in the two spinel phases. Within the spinel structure, Zn does not obtain any crystal field stabilization energy in octahedral sites and therefore it strongly favors the tetrahedral sites occupied by most divalent cations [*Dunitz and Orgel*, 1957; *Lenaz et al*., 2004; *McClure*, 1957; *Navrotsky and Kleppa*, 1967; *Paktunc and Cabri*, 1995]. Zn is also present in very small quantities in the pyroxene and glass phases in both basalts. Although Zn can occupy either octahedral site in the pyroxene structure it prefers the M2 site [*Brown*, 1982; *Burns*, 1970a].

The two spinel phases in our synthesized basalts also contain the highest concentration of Cr compared to the other phases present. As previously mentioned, at an oxygen fugacity near the FMQ buffer, Cr occurs primarily as Cr^{3+}. Due to its very strong octahedral site preference, Cr^{3+} is always found in octahedral coordination in the spinel structure [*Burns*, 1970a, 1973; *Burns and Burns*, 1975; *Lenaz et al*., 2004; *Murck and Campbell*, 1986; *Paktunc and Cabri*, 1995; *Papike et al*., 2005; *Reynolds*, 2005]. Cr^{2+} does not significantly partition into spinel because it must compete for sites with other divalent cations, such as Fe^{2+}, which are commonly much more abundant [*Hanson and Jones*, 1998; *Murck and Campbell*, 1986]. The spinel structure will be discussed in more detail in a following section.

Cr^{2+} can, however, partition into olivine where it occupies the more distorted M1 site [*Burns*, 1970a; *Murck and Campbell*, 1986]. It has been found that Cr concentrations in olivine increase with decreasing oxygen fugacity [*Murck and Campbell*, 1986]. This may explain why the olivine in our plagioclase-bearing basalt, which was crystallized at a lower oxygen fugacity, contains Cr, while the olivine in the plagioclase free basalt

contains none. Consequently, the concentration of Cr in solution F is higher than in solution B. As Cr^{2+} is stabilized in distorted octahedral sites [*Burns and Burns,* 1975] it prefers the M2 sites in pyroxene while Cr^{3+} occupies the M1 sites [*Burns,* 1970a, 1970b]. However, Cr is only present in very small amounts in our pyroxenes.

Although Ni occurs in spinel and pyroxene, it is believed that olivine is the reason for its high abundance in solution. Olivine is the fastest dissolving mineral phases in our basalts so it is reasonable that Ni is more abundant than Zn and Cr in solution. The next most abundant is Zn, most likely due to the small amount that is contained in olivine and due to its position in the most mobile pyroxene site (see above). Excluding experiment F, Cr appears to be the least mobile of the three trace elements (Figure 8b). This is most likely due to the site it occupies in the spinel structure where it tends to be less readily mobilized (see below). The basalt utilized in experiment F had higher abundances of Cr than Zn in the olivine (most likely due to the lower oxygen fugacity in which it crystallized), which explains the higher abundance of Cr in solution.

3.3 Chromite - Results

The compositions of both chromites were determined by electron microprobe and can be seen in Table 4. It is important to note that these chromites may also contain small amounts of Fe^{3+} as calculated cation to oxygen ratios were slightly greater than 3:4. The electron microprobe was also employed along with XRD patterns obtained from both chromites to determine the presence of other phases. Small amounts of olivine were found in the chromite sample referred to as CW. Although attempts were made to

exclude the olivine phase from alteration experiments, it is possible that small amounts were included. The C6 sample was found to be free of other phases.

3.4 Chromite Alteration Experiments - Results and Interpretations

Discussed below are the results for the experiments performed on the two chromites C6 and CW. The solution chemistry will be followed by a discussion and interpretation of the data. Full solution analyses for each experiment can be found in Appendix B.

3.4.1 Chromites - Solution Chemistry

In all experiments performed, Mg and Fe are the most abundant elements in solution (Appendix B8-B11). The experiments that utilized the CW chromite have much higher concentrations of Mg and Fe in solution than the solutions reacted with C6. This may be explained by small amounts of olivine that were included in the CW experiments as mentioned above. The next most abundant element in the C6 experiments is Al, while Cr is the next most abundant element in the CW solutions. The variation of these two elements in the solution chemistry appears to reflect the differing concentrations of Al and Cr in the unweathered chromites (Table 4). The remaining elements that are present in low quantities in both chromites include Mn, Ti, Ni, and Zn. Consequently, these

elements are not abundant in any of the experiments solution chemistry and in some cases they are approaching detection limits.

Comparing element ratios in solution to those in the original chromites further help to better understand how these chromites are dissolving. CW shows similar results to C6 in the element ratio graphs; however, due to the higher abundances of Mg and Fe in CW solutions their results do differ slightly and therefore will not be discussed. Figure 11a shows divalent element ratios, which appear to be dissolving in near to stoichiometric proportions, except for the Fe/Mg ratio where Mg concentrations are higher than those of Fe. The Al/Cr ratio shown in Figure 11b suggests that trivalent elements are not being released into solution in a stoichiometric manner relative to one another. When comparing elements of different valences, it appears as if divalent cations are being released preferentially relative to trivalent ones (Figure 11b).

After the completion of the experiments the remaining materials in those experiments whose solutions fully evaporated where analyzed. The fully evaporated samples included all of those with a staring pH of 2. No secondary phases were identified with XRD analyses. SEM/EDS analyses did identify a few phases (Figure 12), however, the hydration states of these phases is unknown. Mg sulfates were identified in all of the experiments that were analyzed. A Fe sulfate phase was also identified in the experiment with chromite C6 that had a 10:1 water:rock ratio and a starting pH of 2 (C6-10-pH2). Fe sulfate cement, seen in Figure 12b, was found between the chromite grains in experiment C6-100-pH2. In experiment CW-10-pH2, a Fe oxide phase was identified that also had high concentrations of Cr (Figure 12d inset).

3.4.2 Chromites - Interpretation and Discussion

Chromite belongs to the spinel group, which has the general formula XY_2O_4. There are two end members that exist in the spinel structure depending on the distribution of cations. The "normal" spinel structure contains the two trivalent cations in the octahedral sites ($X(Y_2)O_4$). When the trivalent cations are distributed between both the tetrahedral and octahedral sites ($Y(XY)O_4$) the structure is referred to as "inverse" [*Murck and Campbell*, 1986; *Sack*, 1982]. It is important to understand which sites elements occupy within a given structure as it has a direct affect on the rate at which they are released. For example Al is an element that can occupy either tetrahedral and/or octahedral sites in many different phases. However, octahedrally coordinated Al ions are more rapidly leached that Al that occupies tetrahedral sites [*Casey and Bunker*, 1990].

There appears to be no debate about the sites that Zn^{2+} and Cr^{3+} occupy within the spinel structure. As mentioned previously, Zn^{2+} strongly favors the tetrahedral sites [*McClure*, 1957; *Navrotsky and Kleppa*, 1967; *Paktunc and Cabri*, 1995]. Mn^{2+} also occupies the tetrahedral site in chromite [*Henderson et al*., 2007; *Reynolds et al*., 2005], most likely due to its inability to compete with trivalent ions for the octahedral sites. Cr^{3+} has the highest octahedral site preference of any of the transition metals [*Murck and Campbell*, 1986, Oze et al., 2004] and as a result is always assumed to occupy the octahedral site. Consequently, chromites tend to acquire a completely "normal" spinel structure [*Murck and Campbell*, 1986; *Navrotsky and Kleppa*, 1967; *Reynolds*, 2005; *Verwey and Heilmann*, 1947].

However, some Ni bearing chromites have been known to deviate from "normal" distribution as Ni^{2+} also has a large octahedral site preference [*Henderson et al.*, 2007; *Navrotsky and Kleppa*, 1967]. On the other hand, Ni has been found to occupy tetrahedral

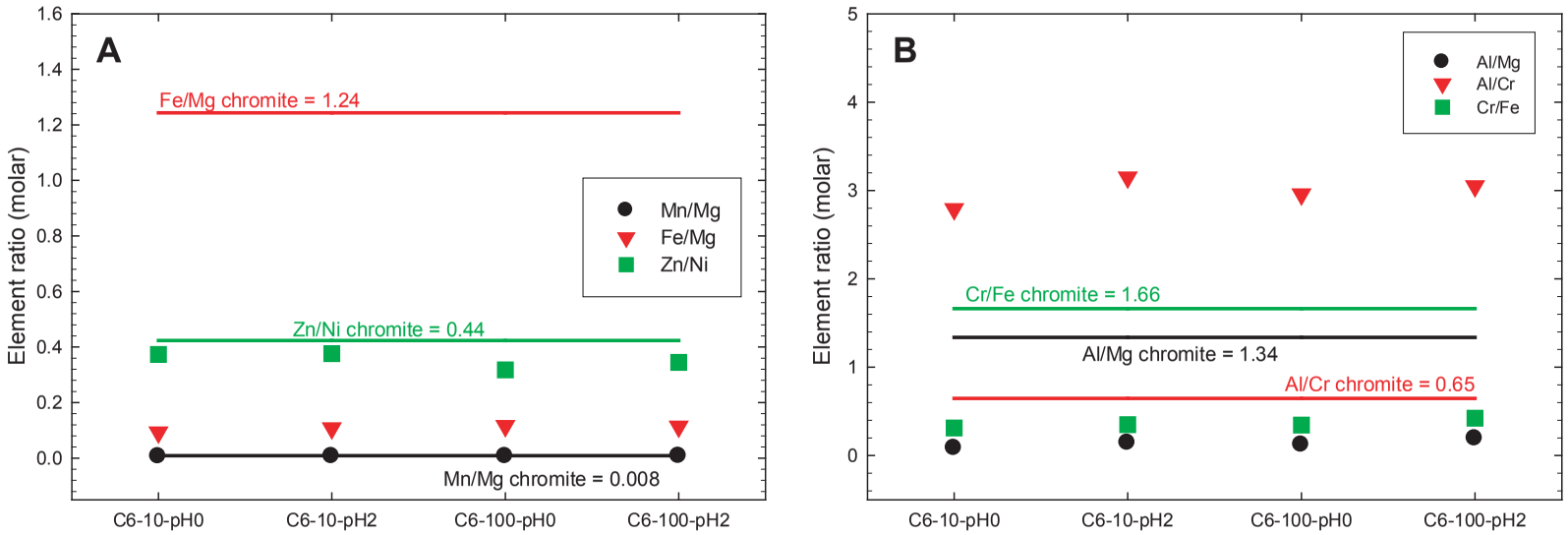

Figure 11. (a) Divalent element to element ratios at 1180 hours for all the C6 experiments performed. (b) Trivalent to divalent element ratios and trivalent element ratio at 1180 hours for all the C6 experiments performed.

sites in the presence of large amounts of Cr^{3+} [*Reynolds*, 2005]. A study by *Lenglet et al.* [1987] found that Ni will always occupy octahedral sites if the total Cr accounts for less than one third of the total cations in the spinel. This suggests that Cr occupies less than half of the octahedral sites leaving more sites available for Ni. In the two chromites used in this study, Cr accounts for much more than one third the total metal-ions indicating Ni is mainly in tetrahedral coordination. Work by *McClure* [1957] indicates that Al^{3+} is also able to compete with Ni^{2+} for octahedral sites. Other studies also suggest a "normal" spinel structure for Ni bearing chromites [*Dunitz and Orgel*, 1957; *Verwey and Heilmann*, 1947] and therefore Ni is believed to be contained in the tetrahedral sites.

Similar to Ni, there is some debate over the structural positions that Fe, Mg, and Al occupy. *Paktunc and Cabri* [1995] argue that Fe^{2+} is always tetrahedrally coordinated in chromite, while Mg and Al^{3+} are the only major cations present in both sites. On the other hand, *McClure* [1957] argues that Fe^{2+} has a small octahedral site preference but can be displaced by Al^{3+} into tetrahedral interstices. *Da Silva et al*. [1980] and *Fatseas et al*. [1976] argue that Fe^{3+} and Fe^{2+} are distributed between both tetrahedral and octahedral sites in the chromite structure. According to other work on spinels, Fe^{3+} is believed to have a small tetrahedral site preference but can be easily displaced if other competitors, such as Zn^{2+}, are present [*Natvrotsky and Kleppa*, 1967; *Verwey and Heilmann*, 1947]. Increased temperature has also been proposed as a cause for cation disorder among sites [*Lenaz et al.*, 2004; *Osborne et al.*, 1981]. However, others argue that all Al- and Cr-bearing spinels have "normal" structures, suggesting that all divalent cations are in the tetaherdral sites and all trivalent cations occupy the octahedral sites [*Garnier et al.*, 2008; *Irvine*, 1965; *Jackson*, 1969; *Osborne et al*., 1981].

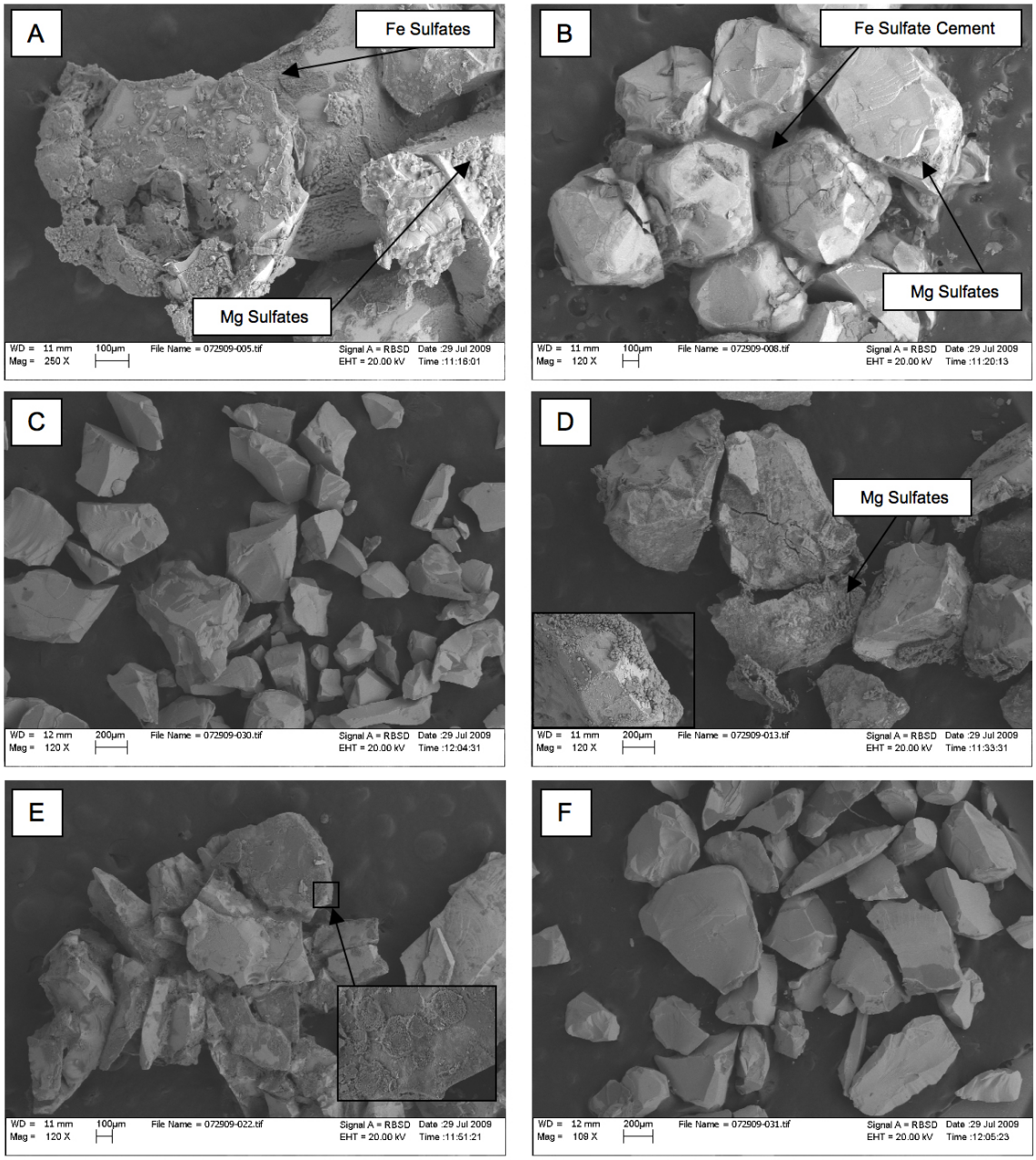

Figure 12. Scanning electron micrographs of chromites: (a) C6-10-pH2, (b) C6-100-pH2, (c) unreacted C6, (d) CW-10-pH2 (inset: Fe-Cr oxides covering a chromite grain), (e) CW-100-pH2 (inset: Mg Sulfate), and (f) unreacted CW.

With so much uncertainty over which sites these elements occupy it is challenging to properly understand the manner in which chromite dissolves. Ultimately, the composition of the chromite strongly influences the cation distribution among the tetrahedral and octahedral sites. As Cr is such a large component in our spinels it will occupy a large majority of the octahedral sites. Consequently, we will assume a mostly "normal" structure while discussing element release from our chromites.

The observation that divalent cations appear to have been released preferentially to trivalent cations might seem contradictory assuming the sites they occupy in the "normal" spinel structure. As we discussed in the previous sections, the method in which glass and other minerals dissolve involves the initial release of cations from the larger octahedral sites, while the elements in the tetrahedral sites have stronger bonds and are more resistant, acting as the material's framework. However, it is apparent that the same mechanism is controlling element release as in the basalt experiments when bond strengths are taken into consideration.

The crystal field theory and octahedral site preference energies may provide an explanation for the incongruent dissolution we observe. Crystal field stabilization energy (CFSE) is the net energy gained by an ion's bonding d-electrons due to complex formation and it indirectly describes an ion's stability within the crystal structure [*Oze et al.*, 2004]. Octahedral site preference energy (OSPE) is the difference between the crystal field stabilization energy of the tetrahedral and octahedral sites [*Oze et al.*, 2004]. The more negative these energies are the harder it is to remove the ion due to the stronger bonds that are formed with the surrounding oxygens in this site. For example, Cr^{3+} has

the most negative CFSE and OSPE of any of the transition metals and as a result would be one of the last ions to be removed from the spinel structure [*Oze et al*., 2004].

In addition, according to *Lavina et al*. [2002] and *Lenaz et al.* [2004], modifications have to be made within the chromite's structure to accommodate various cation distributions. Tetrahedral bond distances may have to adjust in order for certain cations to occupy the octahedral sites [*Lavina et al*., 2002]. The distortion in the structure to accommodate various cations may influence the manner in which the cations are released.

These theories support the observations made for our chromite alteration experiments. The trivalent ions that have very strong octahedral site preference (e.g. Cr and Al) are not as abundant in solution as the divalent ions. Two instances are displayed in Figure 11b where the elements Mg and Fe were released in much higher abundances than Al and Cr . Another example that is not shown in Figure 11 is the Ni to Al ratio. Even though both elements have large octahedral site preferences, Ni is much more abundant in solution than Al. However, Al has a greater octahedral site preference [*Burdett et al*., 1982] and with such considerable amounts of Al and Cr in these chromites Ni most likely gets forced to occupy tetrahedral sites.

When comparing elements of the same valence it is also necessary to consider their site preferences. Mn^{2+} and Mg also have very little ability to compete with elements that have very strong octahedral site preference. Therefore they are both believed to occupy tetrahedral site and are consequently released in close to stoichiometric proportions (Figure 11a). Ni appears to have been released in slightly higher concentrations than Zn. Zn has a strong tetrahedral site preference (see above) and is

expected to be more stable within these sites than Ni. The preferential release of Mg relative to Fe (Figure 11a) may be explained by the assumption that some amount of Fe in the chromites is trivalent Fe. Al, having a smaller octahedral site preference than Cr, was released in greater proportions.

Chapter 4

Discussion and Conclusions

4.1 PFS Basalt Experiments

The mineral assemblage contained in our basalt (Table 6) has been predicted for basalts with Martian compositions using the MELTS program [*McSween et al*., 2004, 2006]. Varying abundances of these minerals have also been identified in rocks and soils on the surface.

Previous alteration studies performed on basaltic materials have also found results similar to ours. Studies on basaltic glass have shown that the initial step in glass dissolution involves the rapid preferential release of alkali and alkaline earth metals. These network modifying elements are removed by a series of metal for proton exchange reactions that occur at the surface [*Casey and Bunker,* 1990; *Gislason and Oelkers*, 2003; *Jantzen and Plodinec*, 1984; *Oelkers and Gislason*, 2001; *White et al*., 1984]. In the current study, the rate of element release was proportional to the element valency, which confirms the occurrence of this surface reaction. A leached layer depleted in the modifying elements and enriched in the glass forming elements, such as Si, was formed in our experiments similar to those found in previous studies [*Doremus et al.*, 1983; *Oelkers and Gislason*, 2001; *Tosca et al.*, 2004; *Wolff-Boenisch et al*., 2004].

The next step in the dissolution of glass involves the destruction of its framework. After the network modifiers are removed, a partial removal of Al atoms occurs by Al-

proton exchange [*Oelkers and Gislason*, 2001]. The rest of the network-forming metals are then slowly detached from a partially liberated glass network [*Bouska*, 1993; *Gislason and Oelkers*, 2003; *Oelkers and Gislason*, 2001]. The liberated Si may be precipitated as amorphous silica, a phase common in our experiments.

The composition of the basaltic glass also plays a major role in its dissolution [*Bouska*, 1993; *Gislason and Oelkers*, 2003; *Glass*, 1984; *Jantzen and Plodinec*, 1984; *Oelkers*, 2001; *Oelkers and Gislason*, 2001]. Higher concentrations of Si produce increased amounts of bridging oxygens and consequently a stronger framework. Dissolution rates also depend on the concentrations of other cations such as Fe^{3+} and Al, which can fill in for Si in the network forming sites. The breaking of the Al-O and Fe-O bonds is quicker than the Si-O bonds and therefore the framework of the glass dissolves faster when the abundance of these elements increases [*Oelkers and Gislason*, 2001]. The concentration of modifiers also has an affect on the dissolution rates as their incorporation into the structure results in bond breakage between the Si and O [*Bouska*, 1993].

Under conditions that are similar to those found on Earth, olivine is the most susceptible mineral to dissolution, followed by plagioclase, pyroxene and the iron oxides [*Eggleton et al*., 1987; *Nesbitt and Wilson*, 1992]. Olivine is also readily altered under Martian-like conditions and as a result Mg and Fe dominate the solution chemistry. Accordingly, Mg and Fe sulfates, like those found in the current study, are commonly produced [*Golden et al*., 2005; *Tosca et al.*, 2004]. Similar studies also found that pyroxene and plagioclase are responsible for the large abundances of Al and Ca in solution, which results in Al and Ca sulfates [*Banin et al*., 1997; *Golden et al*., 2005;

Tosca et al., 2004]. Large amounts of amorphous silica that were found in this study are similar to phases found in other Martian analog alteration studies [*Baker et al*., 2000; *Golden et al.,* 2005; *Morris et al.,* 2000b; *Tosca et al.,* 2004].

The secondary minerals identified in these experiments are also in good agreement to those believed to have been identified on the Martian surface. High Si deposits interpreted as amorphous silica have been detected at both MER sites [*Glotch and Bandfield,* 2006; *Haskin et al.*, 2005; *Ming et al*., 2006; *Squyres et al*., 2008]. A variety of secondary Fe oxides have also been identified at both Gusev Crater and Meridiani Planum [*Christensen et al.,* 2004; *Klingelhofer et al.,* 2004; *Morris et al.,* 2006a] as well as in Martian meteorites [*Bridges and Grady,* 2000]. Evidence for Ca-sulfates, such as gypsum and anhydrite, has also been found in Martian meteorites [*Bridges and Grady*, 2000] and on the surface in layered terrains and in the northern polar region [*Gendrin et al*., 2005*; Langevin et al.,* 2005]. Fe- and Mg-rich sulfates including jarosite and kieserite have also been identified [*Gendrin et al.,* 2005; *Klingelhofer et al.,* 2004; *Ming et al*., 2006; *Morris et al*., 2006a; *Clark et al*., 2005].

4.2 Chromite Experiments

There have been previous studies on chromium mobility due to chromite dissolution under a variety of conditions [*Garnier et al.,* 2008; *Geveci et al.,* 2002; *Hey,* 1999; *Oze et al.,* 2004; *Ulmer*, 1974; *Vardar et al*., 1994]. The general conclusion of these works is that chromite, although very resistant, will weather and alteration increases

with increasing temperature and is at a minimum under intermediate pH conditions. *Vardar et al*. [1994] found that metal release from the chromite structure is stiochiometric. However, other studies report non-stoichiometric release of cations [*Hey*, 1999, *Oze et al.*, 2004]. *Oze et al*. [2004] found that Al and Mg are released preferentially from the chromite structure compared to Cr, which is in agreement with our findings.

4.3 Trace Elements

On the Earth's continental crust granitic rocks and their metamorphic and sedimentary products dominate the surface. As this is where most surficial processes occur, the chemistry of terrestrial soils, sediments, and waters are controlled by weathering process that affect more felsic glasses and minerals, such as feldspars. Consequently, the abundances of Ni, Zn, and Cr in the terrestrial upper crust are low (Table 8). Most aqueous processes on Earth occur in the intermediate pH range, where the solubility of these trace elements is at a minimum. The very low crustal abundances and low mobility of Ni, Zn, and Cr under the conditions commonly found on Earth results in low abundances of these elements in secondary terrestrial minerals.

In contrast, Mars is a basaltic planet and the bulk composition of the crust is estimated to have much higher abundances of Ni, Zn, and Cr (Table 8). Mafic glasses and mafic minerals, such as olivine, pyroxene, Fe-Ti oxides, and plagioclase, dominate the surface and consequently these phases control the fluid chemistry. The low pH conditions, believed to have been active at some point during the Martian past, allow

elements that would not be released under more moderate conditions to be mobilized. Ni, Zn, and Cr are concentrated in theses mafic phases and are more soluble under these lower pH conditions. As the current study has shown, these trace elements are much more mobile under Martian conditions than those conditions common on Earth, making them readily available for secondary materials, such as evaporative processes.

Table 8. Crustal concentrations of trace elements for Earth and Mars

Element (ppm)	Earth[1]	Mars[2]
Ni	44	337
Zn	71	320
Cr	83	2600

Data taken from *Taylor and McLennan* [2009].
[1] Chemical composition of the upper continental crust
[2] Estimate of bulk crustal composition

A few studies have looked at the mobility of the trace elements Ni, Zn, and Cr under various conditions pertaining to Earth [*Aiuppa et al*., 2000a, 2000b; *Das and Krishnaswami*, 2007; *Eggleton et al.,* 1987; *Elbaz-Poulichet et al.,* 1999; *Hocella et al.,* 1999; *Neel et al.,* 2007; *Soubrand-Colin et al.,* 2005]. Although the mobility of each trace element varies from study to study, the general conclusion is that Ni and Zn are more mobile than Cr due to their concentrations in more readily weathered minerals. Some studies report Cr to be essentially immobile due to its preferential location within weather

resistant minerals, while others report some degree of mobility. The contradictory findings can most likely be attributed to the various basalt compositions and extent of alteration in each study.

The small quantities of these elements that are released from alteration processes may have a variety of fates. According to *Nesbitt and Wilson* [1992] and *Soubrand-Colin et al.* [2005], Ni and Cr may be incorporated into smectite and Fe-oxyhydroxides. Ni and Zn strongly complexes to carbonate or bicarbonate if there is a large amount of carbonate species present [*Aiuppa et al*., 2000a, 2000b]. Zn can be immobilized by organo-minerals phases [*Latrille et al*., 2003; *Neel et al.*, 2007] or by sorption onto Fe-bearing phases at near neutral pH [*Hudson-Edwards and Edwards*, 2005; *Johnson*, 1986]. The low hydroxyl solubility of Cr^{3+} and its strong retention on soil particles limits its mobility in soils and waters [*Fendorf et al.*, 1995]. However, Cr^{3+} can also be oxidized by manganese oxides to Cr^{6+}, mainly present in soils as $HCrO_4^-$, which is a highly toxic and soluble species [*Becquer et al*., 2003; *Fendorf et al*., 1995]. Once mobilized during oxidative weathering on Earth, Cr enters the oceans and can be reduced to Cr^{3+} by microbes and Fe^{2+} bearing minerals [*Frei et al*., 2009]. However, the surface of Mars appears to be devoid of organic material and consequently any Cr^{6+} present may not easily revert to the non-toxic trivalent state. Abundant Cr^{6+} on the Martian surface could pose a threat to astronaut health during potential manned missions, especially if it is present in airborne dust.

Many experimental studies have shown that Ni, Zn, and Cr can be incorporated into the structure of Fe oxides and oxyhydroxides. These elements can substitute for Fe in goethite under highly alkaline conditions [*Cornell et al*., 1992; *Gerth*, 1990; *Kaur et al*.,

2009; *Schwertmann*, 1989; *Singh et al*., 2002: *Wells and Gilkes*, 1999; *Wells et al*., 2006]. Under similar conditions, Ni and Cr have also been found to incorporate into the hematite structure [*Sileo et al*., 2007; *Singh et al*., 2000; *Wells and Gilkes*, 1999].

Ni and Zn have a tendency to be adsorbed on clay and oxide surfaces within pH ranges of 3 to 9 [*Arai*, 2008; *Beukes et al*., 2000; *Koppelmann and Dillard*, 1975; *Madrid et al.*, 1991; *Puls et al*., 1988; *Scheidegger et al*., 1997; *Srivastava and Srivastava*, 1990]. Many studies have looked at the adsorption of Ni and Zn onto calcite [*Lakshtanov and Stipp*, 2007; *Zachara et al*., 1988, 1991] and clay minerals such as pyrophyllite, kaolinite, gibbsite and montmorillonite [*Bradl*, 2004; *Davidson et al*., 1991; *Koppelman and Dillard*, 1975, 1977; *Nachtegaal and Sparks*, 2004; *Scheidegger et al*., 1996, 1997; *Singh et al*., 2001]. Cr^{6+} can also be adsorbed by a variety of oxides and clays [*Bradl*, 2004; *Zachara et al*., 1987].

Although these studies pertained to Earth-like conditions, many can also be related to those minerals found on Mars. Hematite and goethite have been found at both landing sites and may be possible sinks for Ni, Zn and Cr. The soils on the Martian surface that are dominated by hematite spherules have a strong Ni-Fe correlation [*Yen et al.*, 2005 and 2006]. Mobilized Ni could be substituting for Fe during the formation of the concretions or Ni may be adsorbing onto the surface of the hematite after its formation.

According to *Clark et al*. [2007b] Ni, Cr and Zn can substitute for Al in the montmorillonite structure, which is one of many clay minerals believed to be present on the Martian surface. Carbonates have also been identified in Martian meteorites and as a possible phase in Martian dust. Ni, Zn and Cr can also get incorporated into the structure of many sulfates [*Jambor et al.*, 2000], which dominate the Martian surface.

4.4 Conclusions

In glass, trace element release rates are controlled by their coordination within the glass structure. Tetrahedrally coordinated elements are strongly covalently bonded and make up the framework of the glasses structure. Octahedrally coordinated elements modify the structure and are held less tightly during dissolution. In some cases the site an ion takes is dependent on the other cations that are present in close proximity. As a result, the composition of the glass has a large influence on its dissolution. In basalt however, their mineralogical setting determines the rate in which trace elements will be leached.

Under the oxidation conditions of terrestrial magmas Cr occurs predominantly as Cr^{3+} [*Calas et al.,* 2006]. Due to its large octahedral site preference, Cr^{3+} always occupies octahedral sites in the structure of glass and minerals. However, on Mars, where oxygen fugacities may be lower than those on Earth, some amount of Cr^{2+} is likely present in the basalts [*Papike et al.,* 2005].

As Cr^{2+} is not retained on quenching to glass due to an electron exchange reaction [*Berry et al.,* 2006] any additional Cr^{2+} will have little affect on the release of Cr from glass. On the other hand, the amount of Cr^{2+} present in crystalline basalt will have a large influence on Cr mobility, as was observed in our study. The basalt that crystallized at a lower oxygen fugacity (utilized in experiment F) had Cr present in its olivine, which is the fastest phase to alter. The basalt that crystallized at a higher oxygen fugacity did not contain Cr in its olivine; instead most of its Cr was contained in the more resistant phases, such as chromite. Consequently, experiment F had higher concentrations of Cr in solution.

The presence of other elements has a large influence on the site Ni occupies within the structure of glass and many mineral phases. In glass, Ni may occur as a tetrahedrally or octahedrally coordinated element depending on the abundance of low or high field strength cations. In mineral phases, like chromite for example, Ni may have to compete with other elements for certain sites within the structure. However, because their mineralogical setting controls the mobility of trace elements, compositional variations will have a greater affect on glass. In other words, the site that Ni occupies within the spinel structure will have little significance if Ni-bearing olivine is present, as olivine will be altered considerably faster, whereas Ni in glass will be released depending on the site it occupies within the structure. Ni was found to be readily mobile in both the glass and crystalline experiments performed in this study, most likely due to its network-modifying position in the glass and the presence of Ni-bearing olivine in our basalt.

Similar to Ni, some argue that the coordination Zn occupies within the structure of glass will depend on the glasses composition. Others argue that Zn will always occupy the tetrahedral site. In this study Zn was not readily weathered from glass leading to the conclusion that most of the Zn was tetrahedrally coordinated. Similar to the other trace elements in the basalt experiments, Zn was released according to its mineralogical setting. Zn was present in olivine but was not as abundance as Ni and consequently the concentrations of Zn in solution were lower. The majority of Zn resided in the glass and the more resistant oxides minerals.

This study has shown that the trace elements Ni, Zn and Cr can in fact be mobilized from basalt under low pH conditions. Once mobilized, these trace elements would most likely be available in solution during the formation of secondary minerals.

Anomalous concentrations of Ni, Zn and Cr on Mars could be due to enrichments in these minerals. This does not however rule out the addition of these elements from other sources such as a meteoritic component or volcanic condensates.

References

Aiuppa, A., P. Allard, W. D'Alessandro, A. Michel, F. Parello, M. Treuil, and M. Valenza (2000a), Mobility and fluxes of major, minor and trace metals during basalt weathering and groundwater transport at Mt. Etna volcano (Sicily), *Geochim. Cosmochim. Acta*, *64*, 1827-1841.

Aiuppa, A., G. Dongarra, G. Capasso, and P. Allard (2000b), Trace elements in the thermal groundwaters of Vulcano Island (Sicily), *J. Volcanol. Geotherm. Res.*, *98*, 189-207.

Andersen, D. J., D. H. Lindsley, and P. M. Davidson (1993), QUILF: A Pascal program to assess equilibria among Fe-Mg-Mn-Ti oxides, pyroxenes, olivine, and quartz, *Comput. Geosci.*, *19*, 1333-1350.

Arai, Y. (2008), Spectroscopic evidence for Ni(II) surface speciation at the iron oxyhydroxides-water interface, *Environ. Sci. Technol.*, *42*, 1151-1156.

Arvidson, R. E., et al. (2006), Overview of the Spirit Mars Exploration Rover Mission to Gusev Crater: Landing site to Backstay Rock in the Columbia Hills, *J. Geophys. Res.*, *111*, E02S01, doi:10.1029/2005JE002499.

Baker, L. L., D. J. Agenbroad, and S. A. Wood (2000), Experimental hydrothermal alteration of a martian analog basalt: Implications for martian meteorites, *Meteorit. Planet. Sci.*, *35*, 31-38.

Banin, A., F. X. Han, I. Kan, and A. Cicelsky (1997), Acidic volatiles and the Mars soil, *J. Geophys. Res.*, *102*(E6), 13341-13356, doi:10.1029/97JE01160.

Becquer, T., C. Quantin, M. Sicot, and J. P. Boudot (2003), Chromium availability in ultramafic soils from New Caledonia, *Sci. Total Environ.*, *301*, 251-261.

Berry, A. J., Neill, H. S., Scott, D. R., Foran, G. J., and Shelley, J. M. G. (2006), The effect of composition on Cr^{2+}/Cr^{3+} in silicate melts, *Am. Mineral.*, *91*, 1901-1908.

Beukes, J. P., E. W. Giesekke, and W. Elliot (2000), Nickel retention by goethite and hematite, *Miner. Eng.*, *13*, 1573-1579.

Blum, A. E., and L. L. Stillings (1995), Feldspar dissolution kinetics, in *Chemical Weathering Rates of Silicate Minerals*, edited by A. F. White and S. L. Brantley, pp. 291-351, Mineral. Soc. of Am., Washington, D.C.

Bouska, V. (1993), *Natural Glasses*, Ellis Horwood, New York.

Bradl, H. B. (2004), Adsorption of heavy metal ions on soils and soils constituents, *J. Colloid Interface Sci.*, *277*, 1-18.

Brantley, S. L., and Y. Chen (1993), Chemical weathering rates of pyroxenes and amphiboles, in *Chemical Weathering Rates of Silicate Minerals*, edited by A. F. White and S. L. Brantley, pp. 119-172, Mineral. Soc. of Am., Washington, D.C.

Bridges, J. C., and M. M. Grady (2000), Evaporite mineral assemblages in the nakhlite (Martian) meteorites, *Earth Planet. Sci. Lett.*, *176*, 267-279.

Brown Jr., G. E. (1982), Olivines and Silicate Spinels, in *Orthosilicates*, 2nd ed., edited by P. H. Ribbe, pp. 275-381, Mineral. Soc. of Am., Washington, D.C.

Burdett, J. K., G. D. Price, and S. L. Price (1982), Role of the crystal-field theory in determining the structures of spinels, *J. Am. Chem. Soc.*, *104*, 92-95.

Burns, R. G. (1970a) *Mineralogical Applications of Crystal Field Theory*, Cambridge Univ. Press, New York, 224 pp.

Burns, R. G. (1970b), Site preferences of transition metal ions in silicate crystal structures, *Chem. Geol.*, *5*, 275-283.

Burns, R. G. (1973), Partitioning of transition elements in crystal structures: A provocative review with applications to mantle geochemistry, *Geochim. Cosmochim. Acta*, *37*, 2395-2403.

Burns, R. G. (1987), Ferric sulfates on Mars, *J. Geophys. Res.*, *92*(B4), E570-E574, doi:10.1029/JB092iB04p0E570.

Burns, R. G. (1993), Rates and mechanisms of chemical-weathering of ferromagnesian silicate minerals on Mars, *Geochim. Cosmochim. Acta*, *57*, 4555-4574.

Burns, V. M., and R. G. Burns (1975), Mineralogy of chromium, *Geochim. Cosmochim. Acta*, *39*, 903-910.

Burt, D. M., L. P. Knauth, K. H. Wohletz, and M. F. Sheridan (2008), Surge deposit misidentification at Spor Mountain, Utah and elsewhere: A cautionary message for Mars, *J. Volcanol. Geotherm. Res.*, *177*, 755-759.

Calas, G., L. Cormier, L. Galoisy, and P. Jollivet (2002), Structure-property relationships in multicomponent oxide glasses, *C. R. Chimie*, *5*, 831-843.

Calas, G., O. Majerus, L. Galoisy, and L. Cormier (2006), Crystal field spectroscopy of Cr^{3+} in glasses: Compositional dependence and thermal site expansion, *Chem. Geol.*, *229*, 218-226.

Carr, M. H. (1996), *Water on Mars*, 248 pp., Oxford University Press, New York.

Casey, W. H., and B. Bunker (1990), Leaching of mineral and glass surfaces during dissolution, in *Mineral-Water Interface Geochemistry*, edited by A. F. White and M. F. Hochella, pp. 397-426, Mineral. Soc. of Am., Washington D.C.

Casey, W. H., H. R. Westrich, and G. W. Arnold (1988), Surface chemistry of labradorite feldspar reacted with aqueous solutions at pH = 2, 3, and 12, *Geochim. Cosmochim. Acta*, *52*, 2795-2807.

Christensen, P. R., et al. (2004), Mineralogy at Meridiani Planum from the Mini-TES experiment on the Opportunity Rover, *Science*, *306*, 1733-1739.

Clark, B. C., et al. (2005), Chemistry and mineralogy of outcrops at Meridiani Planum, *Earth Planet. Sci. Lett.*, *240*, 73-94.

Clark, B. C., R. Gellert, D. W. Ming, R. V. Morris, D. W. Mittlefehldt, S. Squyres, and A. Yen (2006), PYTi-NiCr Signatures in the Columbia Hills are present in certain Martian meteorites, *Lunar Planet. Sci. XXXVII, abstract 150*.

Clark, B. C., R. Gellert, A. Yen, and the Athena Science Team (2007a), The Gusev geochemical zoo: compositional diversity of rocks and sediments, from subclass to superclass, with indicators for aqueous activity, Seventh International Mars Conference, abstract 3232, Lunar and Planet. Inst., Pasadena, Calif.

Clark, B. C. et al. (2007b), Evidence for montmorillonite or its compositional equivalent in Columbia Hills, Mars, *J. Geophys. Res.*, *112*, E06S01, doi:10.1029/2006JE002756.

Cormier, L., L. Galoisy, J. M. Delaye, D. Ghaleb, and G. Calas (2001), Short- and medium-range structural order around cations in glasses: A multidisciplinary approach, *C. R. Acad. Sci.,. Ser. IV: Phys.*, Astrophys., *2*, 249-262.

Cornell, R. M., R. Giovanoli, and W. Schneider (1992), The effect of nickel on the conversion of amorphous iron(III) hydroxide into more crystalline iron-oxides in alkaline media, *J. Chem. Technol. Biotechnol.*, *53*, 73-79.

Curti, E., J. L. Crovisier, G. Morvan, and A. M. Karpoff (2006), Long-term corrosion of two nuclear waste reference glasses (MW and SON68): A kinetic and mineral alteration study, *Appl. Geochem.*, *21*, 1152-1168.

Da Silva, E.G., Abras, A., Speziali, N.L., Camara, AOR (1980), Mossbauer-effect study of natural chromites of Brazilian and Philippine, *Appl. Phys.*, *22*, 389-392.

Das, A., and S. Krishnaswami (2007), Elemental geochemistry of river sediments from the Deccan Traps, India: Implications to sources of elements and their mobility during basalt-water interaction, *Chem. Geol.*, *242*, 232-254.

Dasgupta, H. C. (1972), Site preferences of Ni^{2+} and Co^{2+} in clinopyroxene and olivine: A statistical study, *Chem. Geol.*, *9*, 57-65.

Davison, N., W. R. McWhinnie, and A. Hooper (1991), X-ray photoelectron spectroscopic study of cobalt(II) and nickel(II) sorbed on hectorite and montmorillonite, *Clays Clay Miner.*, *39*, 22-27.

Doremus, R. H., Y. Mehrotra, W. A. Lanford, and C. Burman (1983), Reaction of water with glass: Influence of a transformed surface-layer, *J. Mater. Sci.*, *18*, 612-622.

Dunitz, J. D., and L. E. Orgel (1957), Electronic properties of transition-metal oxides. - II: Cation distribution amongst octahedral and tetrahedral sites, *J. Phys. Chem. Solids*, *3*, 318-323.

Eggleton, R. A., C. Foudoulis, and D. Varkevisser (1987), Weathering of basalt: Changes in rock chemistry and mineralogy, *Clays Clay Miner.*, *35*, 161-169.

Elbaz-Poulichet, F., P. Seyler, L. Maurice-Bourgoin, J. L. Guyot, and C. Dupuy (1999), Trace element geochemistry in the upper Amazon drainage basin (Bolivia), *Chem. Geol.*, *157*, 319-334.

Fatseas, G.A, Dormann, J.L., Blanchard, H., (1976), Study of the Fe^{3+}/Fe^{2+} ratio in natural chromites (Fe_x,Mg_{1-x}) $(Cr_{1-y-z}, Fe_y,Al_z)O_4$, J. de Phys., 12, 787-792.

Fendorf, S. E. (1995), Surface-reactions of chromium in soils and waters, *Geoderma*, *67*, 55-71.

Frei, R., C. Gaucher, S. W. Poulton, and D. E. Canfield (2009), Fluctuations in Precambrian atmospheric oxygenation recorded by chromium isotopes, *Nature*, *461*, 250-254.

Gaillard, F., and B. Scaillet (2009), The sulfur content of volcanic gases on Mars, *Earth Planet. Sci. Lett.*, *279*, 34-43.

Galoisy, L., and G. Calas (1991), Spectroscopic evidence for 5-coordinated Ni in $CaNiSi_2O_6$ glass, *Am. Mineral.*, *76*, 1777-1780.

Galoisy, L., and G. Calas (1992), Network-forming Ni in silicate-glasses, *Am. Mineral.*, *77*, 677-680.

Galoisy, L., and G. Calas (1993a), Structural environment of nickel in silicate glass melt systems: Part 1. Spectroscopic determination of coordination states, *Geochim. Cosmochim. Acta*, *57*, 3613-3626.

Galoisy, L., and G. Calas (1993b), Structural environment of nickel in silicate glass melt systems: Part 2. Geochemical implications, *Geochim. Cosmochim. Acta*, *57*, 3627-3633.

Galoisy, L., G. Calas, and G. E. Brown (1995), Intracrystalline distribution of Ni in San Carlos olivine: An EXAFS study, *Am. Mineral.*, *80*, 1089-1092.

Galoisy, L., L. Cormier, S. Rossano, A. Ramos, G. Calas, P. Gaskell, M. Le Grand (2000), Cationic ordering in oxide glasses: The example of transition elements, *Mineral. Mag.*, *64*, 409-424.

Garnier, J., C. Quantin, E. Guimaraes, and T. Becquer (2008), Can chromite weathering be a source of Cr in soils?, *Mineral. Mag.*, *72*, 49-53.

Gellert, R., et al. (2004), Chemistry of rocks and soils in Gusev crater from the alpha particle X-ray spectrometer, *Science*, *305*, 829-832.

Gendrin, A., et al. (2005), Sulfates in Martian layered terrains: The OMEGA/Mars Express view, *Science*, *307*, 1587-1591.

Gerth, J. (1990), Unit-cell dimensions of pure and trace metal-associated goethites, *Geochim. Cosmochim. Acta*, *54*, 363-371.

Gerth, J., G. W. Brummer, K. G. Tiller (1993), Retention of Ni, Zn and Cd by Si-associated goethite, *Z. Pflanz. Bodenkd.*, *156*, 123-129.

Geveci, A., Y. Topkaya, and E. Ayhan (2002), Sulfuric acid leaching of Turkish chromite concentrate, *Miner. Eng.*, *15*, 885-888.

Ghiorso, M. S., and R. O. Sack **(**1995), Chemical mass-transfer in magmatic processes: IV. A revised and internally Consistent thermodynamic model for the interpolation and extrapolation of liquid-soild equilibria in magmatic systems at elevated-temperatures and pressures. *Contrib. Mineral. Petrol.*, 119, 197-212.

Gislason, S. R., and E. H. Oelkers (2003), Mechanism, rates, and consequences of basaltic glass dissolution: II. An experimental study of the dissolution rates of basaltic glass as a function of pH and temperature, *Geochim. Cosmochim. Acta*, *67*, 3817-3832.

Glass, B. P. (1984), Solution of naturally-occuring glasses in the geological environment, *J. Non-Cryst. Solids*, *67*, 265-286.

Glotch, T. D., and J. L. Bandfield (2006), Determination and interpretation of surface and atmospheric Miniature Thermal Emission Spectrometer spectral end-members at the Meridiani Planum landing site, *J. Geophys. Res.*, *111*, E12S0612, doi:10.1029/2005JE002671.

Golden, D. C., D. W. Ming, R. V. Morris, and S. A. Mertzman (2005), Laboratory-simulated acid-sulfate weathering of basaltic materials: Implications for formation of sulfates at Meridiani Planum and Gusev crater, Mars, *J. Geophys. Res.*, *110*, E12S07, doi:10.1029/2005JE002451.

Grotzinger, J. P., et al. (2005), Stratigraphy and sedimentology of a dry to wet eolian depositional system, Burns formation, Meridiani Planum, Mars, *Earth Planet. Sci. Lett.*, *240*, 11-72.

Gustafsson, J. P. (2004), Visual Minteq, version 2.61: A Windows version of MINTEQA2 version 4.0, [WWW document] URL http://www.lwr.kth.se/English/OurSoftware/Vminteq.

Hanson, B., and J. H. Jones (1998), The systematics of Cr^{3+} and Cr^{2+} partitioning between olivine and liquid in the presence of spinel, *Am. Mineral., 83*, 669-684.

Haskin, L. A., et al. (2005), Water alteration of rocks and soils on Mars at the Spirit rover site in Gusev crater, *Nature, 436*, 66-69.

Henderson, C. M. B., Charnock, J. M., and Plant, D. A. (2007), Cation occupancies in Mg, Co, Ni, Zn, Al ferrite spinels: A multi-element EXAFS study, *J. Phys: Condens. Matter*, *19*, pp. 1-25.

Hey, P. V. (1999), The effects of weathering on the UG2 Chromitite reef of the Bushveld Complex, with special reference to the platinum-group minerals, *S. Afr. J. Geol.*, *102*, 251-260.

Hochella, M. F., J. N. Moore, U. Golla, and A. Putnis (1999), A TEM study of samples from acid mine drainage systems: Metal-mineral association with implications for transport, *Geochim. Cosmochim. Acta*, *63*, 3395-3406.

Hudson-Edwards, K. A., and S. J. Edwards (2005), Mineralogical controls on storage of As, Cu, Pb and Zn at the abandoned Mathiatis massive sulphide mine, Cyprus, *Mineral. Mag.*, *69*, 695-706.

Hurowitz, J. A., S . M. McLennan, D. H. Lindsley, and M. A. A. Schoonen (2005), Experimental epithermal alteration of synthetic Los Angeles meteorite: Implications for the origin of Martian soils and identification of hydrothermal sites on Mars, *J. Geophys. Res.*, *110*, E07002, doi:10.1029/2004JE002391.

Hurowitz, J. A., S. M. McLennan, H. Y. McSween, P. A. DeSouza, G. Klingelhofer (2006), Mixing relationships and the effects of secondary alteration in the Wishstone and Watchtower Classes of Husband Hill, Gusev Crater, Mars, *J. Geophys. Res.*, *111*, E12S14, doi:10.1029/2006JE002795.

Irvine, T. N., (1965) Chromian spinel as a petrogenetic indicator, Part 1, Theory. *Can. J. Earth Sci*., *2*, 648-672.

Jackson, E. D., (1969) Chemical variation in co-existing chromite and olivine in chromite zones of the Stillwater complex. *Econ. Geol. Monogr., 4*, 41-71.

Jambor, J. I., D. K. Nordstrom, and C. N. Alpers (2000), Metal-sulfate salts from sulfide mineral oxidation, in *Sulfate Minerals: Crystallography, Geochemistry and Environmental Significance*, edited by C. N. Alpers, J. L. Jambor, and D. K. Nordstrom, pp. 305-350, Mineral. Soc of Am., Washington, D.C.

Jantzen, C. M., and M. J. Plodinec (1984), Thermodynamic model of natural, medieval and nuclear waste glass durability, *J. Non-Cryst. Solids*, *67*, 207-223.

Johnson, C. A. (1986), The regulation of trace element concentrations in river and estuarine waters contaminated with acid-mine drainage: The adsorption of Cu and Zn on amorphous Fe oxyhydroxides, *Geochim. Cosmochim. Acta*, *50*, 2433-2438.

Kaur, N., M. Grafe, B. Singh, and B. Kennedy (2009), Simultaneous incorporation of Cr, Zn, Cd, and Pb in the goethite structure, *Clays Clay Miner.*, *57*, 234-250.

Klingelhofer, G., et al. (2004), Jarosite and hematite at Meridiani Planum from Opportunity's Mossbauer spectrometer, *Science*, *306*, 1740-1745.

Knauth, L. P., D. M. Burt, and K. H. Wohletz (2005), Impact origin of sediments at the opportunity landing site on Mars. *Nature*, 438, 7071

Koppelman, M. H., and J. G. Dillard (1975), An ESCA study of sorbed metal ions on clay minerals, in *Marine Chemistry in the Coastal Environment*, edited by T. M. Church, pp. 186-201, *ACS Symposium Series 18*, Wahington D.C.

Koppelman, M. H., and J. G. Dillard (1977), A study of adsorption of Ni(II) and Cu(II) by clay minerals, *Clays Clay Miner.*, 25, 457-462.

Lakshtanov, L. Z., and S. L. S. Stipp (2007), Experimental study of nickel(II) interaction with calcite: Adsorption and coprecipitation, *Geochim. Cosmochim. Acta*, *71*, 3686-3697.

Langevin, Y., F. Poulet, J. P. Bibring, and B. Gondet (2005), Sulfates in the north polar region of Mars detected by OMEGA/Mars Express, *Science*, *307*, 1584-1586.

Latrille, C., L. Denaix, and I. Lamy (2003), Interaction of copper and zinc with allophane and organic matter in the B horizon of an Andosol, *Eur. J. Soil Sci.*, *54*, 357-364.

Lavina, B., Salviulo, G., and Della Giusta, A. (2002), Cation distribution and structure modeling of spinel solid solutions, *Phys. Chem. Miner.*, *29*, 10-18.

Le Grand, M., A. Y. Ramos, G. Calas, L. Galoisy, D. Ghaleb, and F. Pacaud (2000), Zinc environment in aluminoborosilicate glasses by Zn K-edge extended X-ray absorption fine structure spectroscopy, *J. Mater. Res.*, *15*, 2015-2019.

Lenaz, D., Skogby, H., Princivalle, F., and Halenius, U. (2004), Structural changes and valence states in the $MgCr_2O_4$-$FeCr_2O_4$ solid solution series, *Phys. Chem. Miner.*, *31*, 633-642.

Lenglet, M., A. Dhuysser, and C. K. Jorgensen (1987), Optical-spectra, X-ray photoelectron-spectra and xanes of divalent nickel in mixed spinels $NiFe_2$-$XCrXO_4$, *Inorg. Chim. Acta*, *133*, 61-65.

Madrid, L., E. Diazbarrientos, and M. C. Contreras (1991), Relationships between zinc and phosphate adsorption on montmorillonite and an iron oxyhydroxide, *Aust. J. Soil Res.*, *29*, 239-247.

McClure, D. S. (1957), The distribution of transition metal cations in spinels, *J. Phys. Chem. Solids*, *3*, 311-317.

McLennan, S. M., and J. P. Grotzinger (2008), The Sedimentary Rock Cycle of Mars, in *The Martian Surface: Composition, Mineralogy and Physical Properties*, edited by J. F. Bell, pp. 541-577, Cambridge University Press, New York.

McLennan, S. M., S. Hemming, D. K. McDaniel, and G. N. Hanson (1993), Geochemical approaches to sedimentation, provenance, and tectonics, in *Processes Controlling the Composition of Clastic Sediments*, edited by M. J. Johnson and A. Basu, pp. 21-40, *Geol. Soc. of Am. Spec. Paper, 284*, Boulder, CO.

McLennan, S. M., et al. (2005), Provenance and diagenesis of the evaporite-bearing Burns formation, Meridiani Planum, Mars, *Earth Planet. Sci. Lett.*, *240*, 95-121.

McSween, H. Y., et al. (2004), Basaltic rocks analyzed by the Spirit rover in Gusev Crater, *Science*, *305*, 842-845.

McSween, Y., et al. (2006), Characterization and petrologic interpretation of olivine-rich basalts at Gusev Crater, Mars, *J. Geophys. Res.*, *111*, E02S10, doi:10.1029/2005JE002477.

Merrill, R. B., and P. J. Wyllie (1973), Abdorption of iron by platinum capsules in high-pressure rock melting experiments, *Am. Mineral.* 58, 16-20.

Ming, D. W., et al. (2006), Geochemical and mineralogical indicators for aqueous processes in the Columbia Hills of Gusev crater, Mars, *J. Geophys. Res.*, *111*, E02S12, doi:10.1029/2005JE002560.

Ming, D. W., et al. (2008), Geochemical properties of rocks and soils in Gusev Crater, Mars: Results of the Alpha Particle X-Ray Spectrometer from Cumberland Ridge to Home Plate, *J. Geophys. Res.*, *113*, E12S39, doi:10.1029/2008JE003195.

Morris, R. V., et al. (2000a), Mineralogy, composition, and alteration of Mars Pathfinder rocks and soils: Evidence from multispectral, elemental, and magnetic data on terrestrial analogue, SNC meteorite and Pathfinder samples, *J. Geophys. Res.*, *105*(E1), 1757-1817, doi:10.1029/1999JE001059.

Morris, R. V., et al. (2000b), Acid sulfate alteration products of a tholeiitic basalt: Implications for interpretation of Martian thermal emission spectra, *Lunar Planet. Sci., XXXI*, abstract 2014.

Morris, R. V., et al. (2006a), Mossbauer mineralogy of rock, soil, and dust at Gusev crater, Mars: Spirit's journey through weakly altered olivine basalt on the plains and pervasively altered basalt in the Columbia Hills, *J. Geophys. Res.*, *111*, E02S13, doi:10.1029/2005JE002584.

Morris, R. V., et al. (2006b), Mossbauer mineralogy of rock, soil, and dust at Meridiani Planum, Mars: Opportunity's journey across sulfate-rich outcrop, basaltic sand and dust, and hematite lag deposits, *J. Geophys. Res.*, *111*, E12S15, doi:10.1029/2006JE002791.

Murck, B. W., and I. H. Campbell (1986), The effects of temperature, oxygen fugacity and melt composition on the behavior of chromium in basic and ultrabasic melts, *Geochim. Cosmochim. Acta*, *50*, 1871-1887.

Nachtegaal, M., and D. L. Sparks (2004), Effect of iron oxide coatings on zinc sorption mechanisms at the clay-mineral/water interface, *J. Colloid Interface Sci.*, *276*, 13-23.

Navrotsky. A, and O. J. Kleppa (1967), Thermodynamics of cation distributions in simple spinels, *J. Inorg. Nucl. Chem.*, *29*, 2701-2714.

Neel, C., M. Soubrand-Colin, A. Piquet-Pissaloux, and H. Bril (2007), Mobility and bioavailability of Cr, Cu, Ni, Pb and Zn in a basaltic grassland: Comparison of selective extractions with quantitative approaches at different scales, *Appl. Geochem.*, *22*, 724-735.

Nesbitt, H. W., and R. E. Wilson (1992), Recent chemical-weathering of basalts, *Am. J. Sci.*, *292*, 740-777.

Newsom, H. E., and J. J. Hagerty (1997), Chemical components of the Martian soil: Melt degassing, hydrothermal alteration, and chondritic debris, *J. Geophys. Res.*, *102*(E8), 19345-19355, doi:10.1029/97JE01687.

Oelkers, E. H. (2001), General kinetic description of multioxide silicate mineral and glass dissolution, *Geochim. Cosmochim. Acta*, *65*, 3703-3719.

Oelkers, E. H., and S. R. Gislason (2001), The mechanism, rates and consequences of basaltic glass dissolution: I. An experimental study of the dissolution rates of basaltic glass as a function of aqueous Al, Si and oxalic acid concentration at 25 degrees C and pH=3 and 11, *Geochim. Cosmochim. Acta*, *65*, 3671-3681.

Osborne, M. D., Fleet, M. E., and Bancroft, G. M. (1981), Fe^{2+}-Fe^{3+} ordering in chromite and Cr-bearing spinels, *Contrib. Mineral. Petrol.*, *77*, 251-255.

Oze, C., Fendorf, S., Bird, D. K., and Coleman, R. G. (2004), Chromium geochemistry in serpentinized ultramafic rocks and serpentine soils from the Franciscan Complex of California, *Am. J. Sci.*, *304*, 67-101.

Paktunc, A. D., and L. J. Cabri (1995), A proton- and electron-microprobe study of gallium, nickel and zinc distribution in chromian spinel, *Lithos*, *35*, 261-282.

Papike, J. J., J. M. Karner, and C. K. Shearer (2005), Comparative planetary mineralogy: Valence state partitioning of Cr, Fe, Ti, and V among crystallographic sites in olivine, pyroxene, and spinel from planetary basalts, *Am. Mineral.*, *90*, 277-290.

Pokrovsky, O. S., and J. Schott (2000), Kinetics and mechanism of forsterite dissolution at 25 ºC and pH from 1 to 12, *Geochim. Cosmochim. Acta*, *64*, 3313-3325.

Puls, R. W., and H. L. Bohn (1988), Sorption of cadmium, nickel, and zinc by kaolinite and montmorillonite suspensions, *Soil Sci. Soc. Am. J.*, *52*, 1289-1292.

Reynolds, J. G. (2005), Spinel structure and liquidus temperature relationships in nuclear waste glass, *J. Mater. Sci.*, *40*, 3987-3991.

Rieder, R., et al. (2004), Chemistry of rocks and soils at Meridiani Planum from the alpha particle X-ray spectrometer, *Science*, *306*, 1746-1749.

Roeder, P. L., and I. Reynolds (1991), Crystallization of chromite and chromium solubility in basaltic melts, *J. Petrol.*, *32*, 909-934.

Sack, R. O. (1982), Spinels as petrogenetic indicators: Activity-composition relations at low-pressures, *Contrib. Mineral. Petrol.*, *79*, 169-186.

Scheidegger, A. M., G. M. Lamble, and D. L. Sparks (1996), Investigation of Ni sorption on pyrophyllite: An XAFS study, *Environ. Sci. Technol.*, *30*, 548-554.

Scheidegger, A. M., G. M. Lamble, and D. L. Sparks (1997), Spectroscopic evidence for the formation of mixed-cation hydroxide phases upon metal sorption on clays and aluminum oxides, *J. Colloid Interface Sci.*, *186*, 118-128.

Schmidt, M. E., W. H. Farrand, J. Hurowitz, J. R. Johnson, R. Gellert, and T. J. McCoy **(**2008), Lateral mineralogical and geochemical variation at Home Plate: Implications for fluid flow and hydrothermal alteration, *Lunar Planet. Sci., XXXIX*, abstract 2024.

Schmidt, M. E., et al. (2008). Hydrothermal origin of halogens at Home Plate, Gusev Crater, *J. Geophys. Res.*, *113*, E06S12, doi:10.1029/2007JE003027.

Schott, J., and R. A. Berner (1983), X-ray photoelectron studies of the mechanism of iron silicate dissolution during weathering, *Geochim. Cosmochim. Acta*, *47*, 2233-2240.

Schott, J., and R. A. Berner (1985), Dissolution mechanisms of pyroxenes and olivines during weathering, in *The Chemistry of Weathering*, edited by J. I. Drever, pp. 35-54, Kluwer Acad., Norwell, Mass.

Schwertmann, U., U. Gasser, and H. Sticher (1989), Chromium-for-iron substitution in synthetic goethites, *Geochim. Cosmochim. Acta*, *53*, 1293-1297.

Sileo, E. E., D. P. Daroca, U. A. Barrero, A. L. Larralde, M. S. Giberti, and C. Saragovi (2007), Influence of the genesis on the structural and hyperfine properties of Cr-substituted hematites, *Chem. Geol.*, *238*, 84-93.

Singh, B., D. M. Sherman, R. J. Gilkes, M. Wells, and J. F. W. Mosselmans (2000), Structural chemistry of Fe, Mn, and Ni in synthetic hematites as determined by extended X-ray absorption fine structure spectroscopy, *Clays Clay Miner.*, *48*, 521-527.

Singh, S. P., L. Q. Ma, and W. G. Harris (2001), Heavy metal interactions with phosphatic clay: Sorption and desorption behavior, *J. Environ. Qual.*, *30*, 1961-1968.

Singh, B., D. M. Sherman, R. J. Gilkes, M. A. Wells, J. F. W. Mosselmans (2002), Incorporation of Cr, Mn and Ni into goethite (alpha-FeOOH): Mechanism from extended X-ray absorption fine structure spectroscopy, *Clay Miner.*, *37*, 639-649.

Soubrand-Colin, M., H. Bril, C. Neel, A. Courtin-Nomade, and F. Martin (2005), Weathering of basaltic rocks from the French Massif Central: Origin and fate of Ni, Cr, Zn and Cu, *Can. Mineral.*, *43*, 1077-1091.

Squyres, S. W., and A. H. Knoll (2005), Sedimentary rocks at Meridiani Planum: Origin, diagetiesis, and implications for life on Mars, *Earth Planet. Sci. Lett.*, *240*, 1-10.

Squyres, S. W., et al. (2004), The Spirit Rover's Athena Science Investigation at Gusev Crater, Mars, *Science*, *305*, 794-799.

Squyres, S. W., et al. (2007), Pyroclastic activity at home plate in Gusev Crater, Mars, *Science*, *316*, 738-742.

Squyres, S. W., et al. (2008), Detection of silica-rich deposits on Mars, *Science*, *320*, 1063-1067.

Srivastava, A., and P. C. Srivastava (1990), Adsorption desorption behavior of zinc(II) at iron(III) hydroxide aqueous-solution interface as influenced by pH and temperature, *Environ. Pollut.*, *68*, 171-180.

Stillings, L. L., and S. L. Brantley (1995), Feldspar dissolution at 25°C and pH 3: Reaction stoichiometry and the effect of cations, *Geochim. Cosmochim. Acta*, *59*, 1483-1496.

Taylor, S. R., and S. M. McLennan **(**1985), *The Contintental Crust: Its Composition and Evolution*, 312 pp., Blackwell Scientific, Oxford.

Taylor, S. R., and S. M. McLennan (2009), *Planetary Crusts: Their Composition, Origin, and Evolution*, 400 pp., Cambridge Univ. Press, New York.

Tosca, N. J., and S. M. McLennan **(**2006), Chemical divides and evaporite assemblages on Mars. *Earth and Planet. Sci. Lett.*, 241, 21-31.

Tosca, N. J., S. M. McLennan, D. H. Lindsley, and M. A. A. Schoonen (2004), Acid-sulfate weathering of synthetic Martian basalt: The acid fog model revisited, *J. Geophys. Res.*, *109*, E05003, doi:10.1029/2003JE002218.

Tosca, N. J., S. M. McLennan, B. C. Clark, J. P. Grotzinger, J. A. Hurowitz, A. H. Knoll, C. Schroder, and S. W. Squyres (2005), Geochemical modeling of evaporation processes on Mars: Insight from the sedimentary record at Meridiani Planum. *Earth and Planet. Sci. Lett.*, 240, 122-48.

Ulmer, G. C. (1974), Alteration of chromite during serpentinization in Pennsylvania Maryland district, *Am. Mineral.*, *59*, 1236-1241.

Vardar, E., R. H. Eric, and F. K. Letowski (1994), Acid leaching of chromite, *Miner. Eng.*, *7*, 605-617.

Verwey, E. J. W., and E. L. Heilmann (1947), Physical properties and cation arrangement of oxides with spinel structures: I. Cation arrangements in spinels, *J. Chem. Phys.*, *15*, 174-180.

Wang, A., et al (2008), Light-toned salty soils and coexisting Si-rich species discovered by the Mars Exploration Rover Spirit in Columbia Hills, *J. Geophys. Res.*, *113*, E12S40, doi:10.1029/2008JE003126.

Wells, M. and R. J. Gilkes (1999), Synthetic Ni goethite and hematite: Reproducing hosts for nickel mineralization in Ni-laterites, in *New Approaches to an Old Continent*, edited by G. Taylor and C. Payne, pp. 299-310, *Regolith '98*, Cooperative Research Centre for Landscape Evolution and Mineral Exploration, Wembley, Western Australia.

Wells, M. A., R. W. Fitzpatrick, and R. J. Gilkes (2006), Thermal and mineral properties of Al-, Cr-, Mn-, Ni- and Ti-substituted goethite, *Clays Clay Miner.*, *54*, 176-194.

White, A. F. (1984), Weathering characteristics of natural glass and influences on associated water chemistry, *J. Non-Cryst. Solids*, *67*, 225-244.

Wolff-Boenisch, D., S. R. Gislason, E. H. Oelkers, and C. V. Putnis (2004), The dissolution rates of natural glasses as a function of their composition at pH 4 and 10.6, and temperatures from 25 to 74 ºC, *Geochim. Cosmochim. Acta*, *68*, 4843-4858.

Yen, A. S., et al. (2005), An integrated view of the chemistry and mineralogy of martian soils, *Nature*, *436*, 881-881.

Yen, A. S., et al. (2006), Nickel on Mars: Constraints on meteoritic material at the surface, *J. Geophys. Res.*, *111*, E12S11, doi:10.1029/2006JE002797.

Yen, A. S., et al. (2008), Hydrothermal processes at Gusev Crater: An evaluation of Paso Robles class soils, *J. Geophys. Res.*, *113*, E06S10, doi:10.1029/2007JE002978.

Zachara, J. M., D. C. Girvin, R. L. Schmidt, and C. T. Resch (1987), Chromate adsorption on amorphous iron oxyhydroxide in the presence of major groundwater ions, *Environ. Sci. Technol.*, *21*, 589-594.

Zachara, J. M., J. A. Kittrick, and J. B. Harsh (1988), The mechanism of Zn^{2+}, *Geochim. Cosmochim. Acta*, *52*, 2281-2291.

Zachara, J. M., C. E. Cowan, and C. T. Resch (1991), Sorption of divalent metals on calcite, *Geochim. Cosmochim. Acta*, *55*, 1549-1562.

Zachariasen, W. H. (1932), The atomic arrangement in glass, *J. Am. Chem. Soc.*, *54*, 3841-3851.

Appendix A

Summary of Challenges Encountered During Basalt Synthesis

Previous studies in our lab have successfully synthesized basalts of Martian composition. Our methods are different due to a number of complications we encountered while attempting to follow these previous procedures. Our first complication was the persistence of a spinel phase at 1246° C, the calculated liquidus from the previous study [*Tosca et al.*, 2004]. At first we interpreted this phase to be caused due to the addition of Cr_2O_3 powder in the mix. It was believed there was some Cr_2O_3 remaining at this temperature that nucleated the formation of a metastable chromite. To ensure complete homogenization of the sample higher temperatures were required. The $Au_{80}Pd_{20}$ alloy tubing that had been previously used was not capable of withstanding higher temperatures and had to be replaced with a platinum capsule. As a consequence of the higher temperatures a component of the mix became volatile and the platinum capsules needed to be sealed at both ends. The increased temperature experiments also made it impossible to nucleate plagioclase at lower temperatures, a procedure previously performed by *Tosca et al.* [2004] due to the slow kinetics of plagioclase crystallization in synthetic systems (see the procedures section). As a result a different approach was used in order to synthesize the crystalline basalt at lower temperatures. A new mix was created using uvarovite, a chromium rich garnet, as the source of chromium instead of Cr_2O_3. A larger amount of Fe^o was also added to the new oxide mix in order to replace the significant loss of Fe to the platinum walls during synthesis. Previous experimental studies have also shown absorption of Fe by platinum capsules (e.g., *Merrill and Wyllie*, 1973). After synthesis, the samples were analyzed with the electron microprobe, and it was found that the resulting Ni and Zn contents in the glass were minimal. These two elements have a high affinity for platinum, which might explain their low levels in the melt. As higher temperatures were no longer needed we returned to original procedure using $Au_{80}Pd_{20}$ capsules. The loss of Ni and Zn to the capsule walls was predicted to occur in these capsules as well but to a lesser extent. A series of new mixes were created with increased concentrations of Ni and Zn. The mix with a starting concentration of 10,000 ppm NiO and 5000 ppm ZnO resulted in a glass with 740 ppm NiO and 690 ppm ZnO. The concentration of Fe^o added to the mix was decreased, as the amount of Fe loss is not as substantial in AuPd capsules. Once a glass with this new mix was synthesized and analyzed it became apparent that the metastability of Cr_2O_3 in our previous experiments was not the issue. The lower quantity of Fe° added to the mix and the presence of a spinel phase in this sample led us to believe that the stability of chromite in this run was the result of higher oxygen fugacity.

According to studies on the solubility of chromite in basaltic melts, the chromium content in a melt increases with decreasing oxygen fugacity, at constant temperature. The

increased content of chromium in the melt reflects the increase in the Cr^{2+}/Cr^{3+} ratio with decreasing oxygen fugacity [*Murck and Campbell*, 1986; *Roeder and Reynolds*, 1991]. Since Cr^{2+} prefers the melt relative to Cr^{3+} [*Papike et al.*, 2005], and studies have shown that Cr^{2+} is not readily incorporated into the spinel structure [*Hanson and Jones*, 1998], the stability of chromite is reduced. Other spinel phases would also be destabilized as Fe^{3+} concentrations would also decrease with decreasing oxygen fugacity.

To decrease the amount of chromite in our synthesized basalts we decided to decrease the oxygen fugacity. The first redox buffer we utilized was the CoCoO buffer. The amount of chromite in our basaltic glass decreased but a small amount persisted. The next buffer we tested was the wustite-magnetite buffer which is 3 log units below QFM, our original target oxygen fugacity. Although the samples were not as reduced as the wustite-magnetite buffer we were unable to find any spinel phase under microscope or with the microprobe and the chemical composition was very similar to the target composition. Therefore, we have concluded that our basaltic glass is free of chromite.

Appendix B

Major Element Solution Analysis

Figures B1 through B7 display major and trace element solution data for all PFS basalt alteration experiments discussed. This data includes results for the five different pH solutions (A-E) used in each experiment as well as the calculated pH values. Figures B1 through B3 show results for PFS glass reactions. B4 through B6 show results for PFS crystalline basalt without plagioclase. Figure B7 shows results and calculated pH values for the PFS crystalline basalt experiment with plagioclase that was conducted only with solution F. Figures B8 through B11 show solution chemistry for chromite experiments including both water to rock ratios and both pH solutions used. Figures B8 and B9 show results for C6 experiments and Figures B10 and B11 show results for experiments utilizing CW.

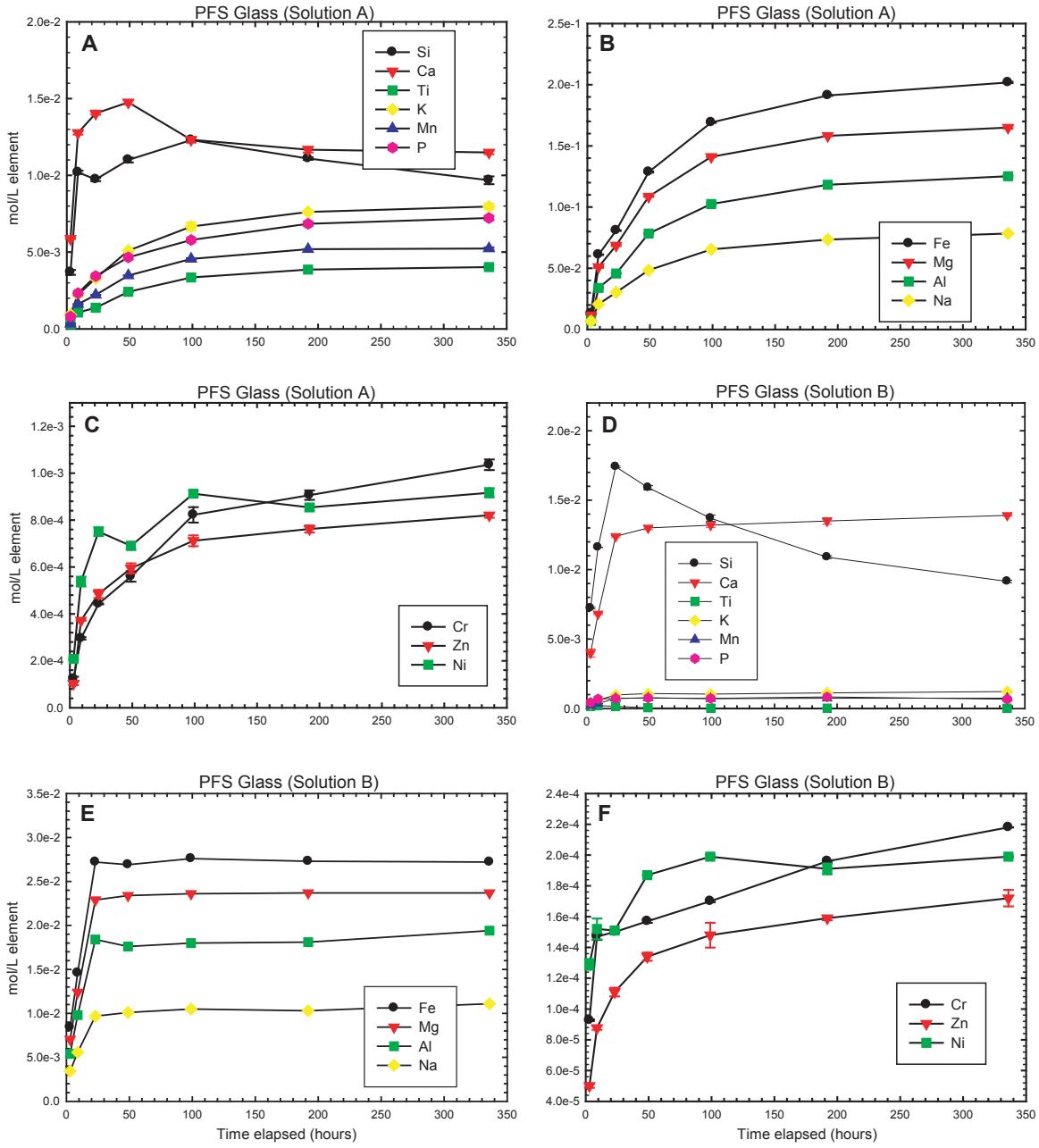

Figure B1. Major and trace element solution concentrations during reaction with PFS glass and (a through c) solution A, (d through f) solution B.

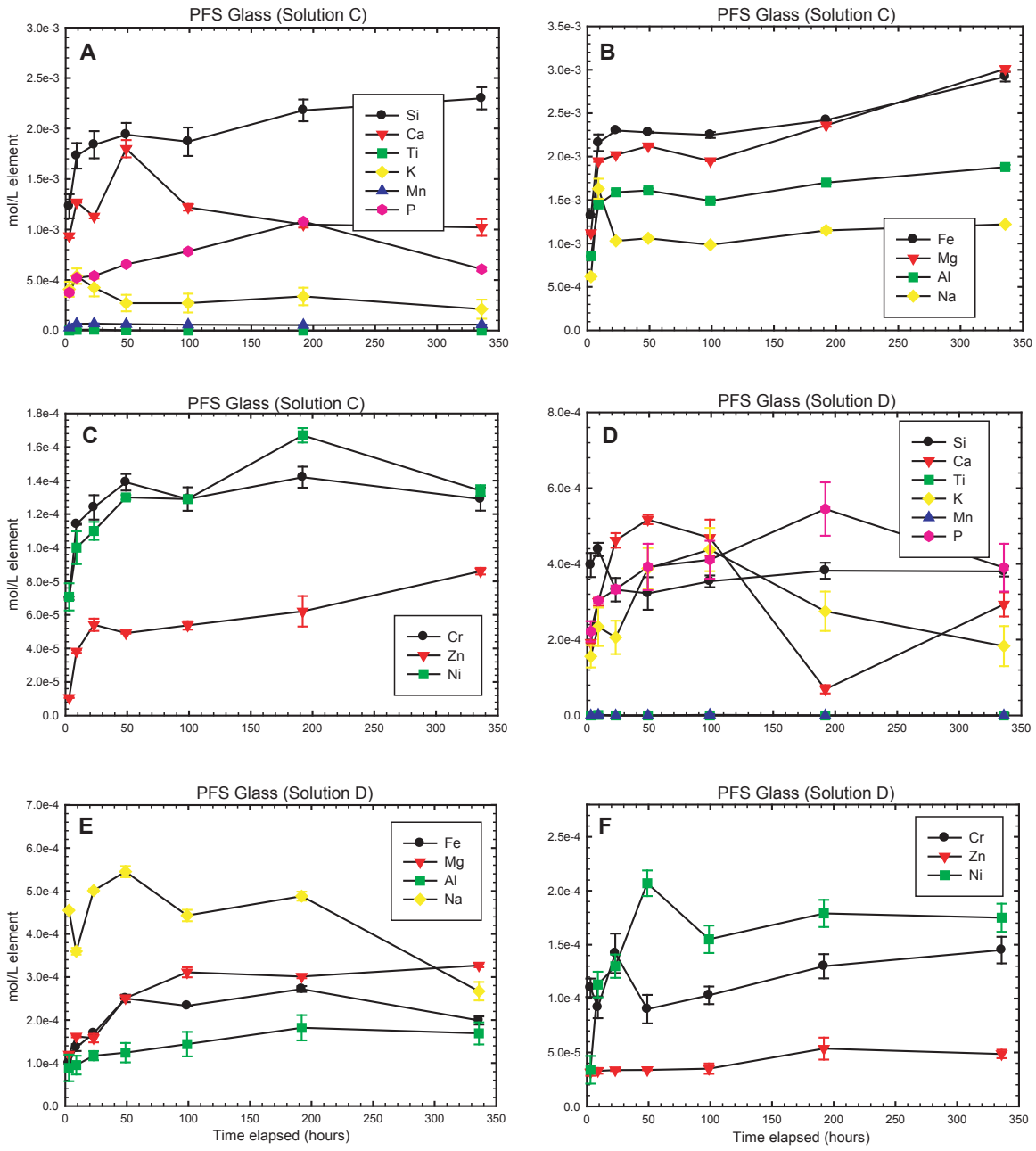

Figure B2. Major and trace element solution concentrations during reaction with PFS glass and (a through c) solution C, (d through f) solution D.

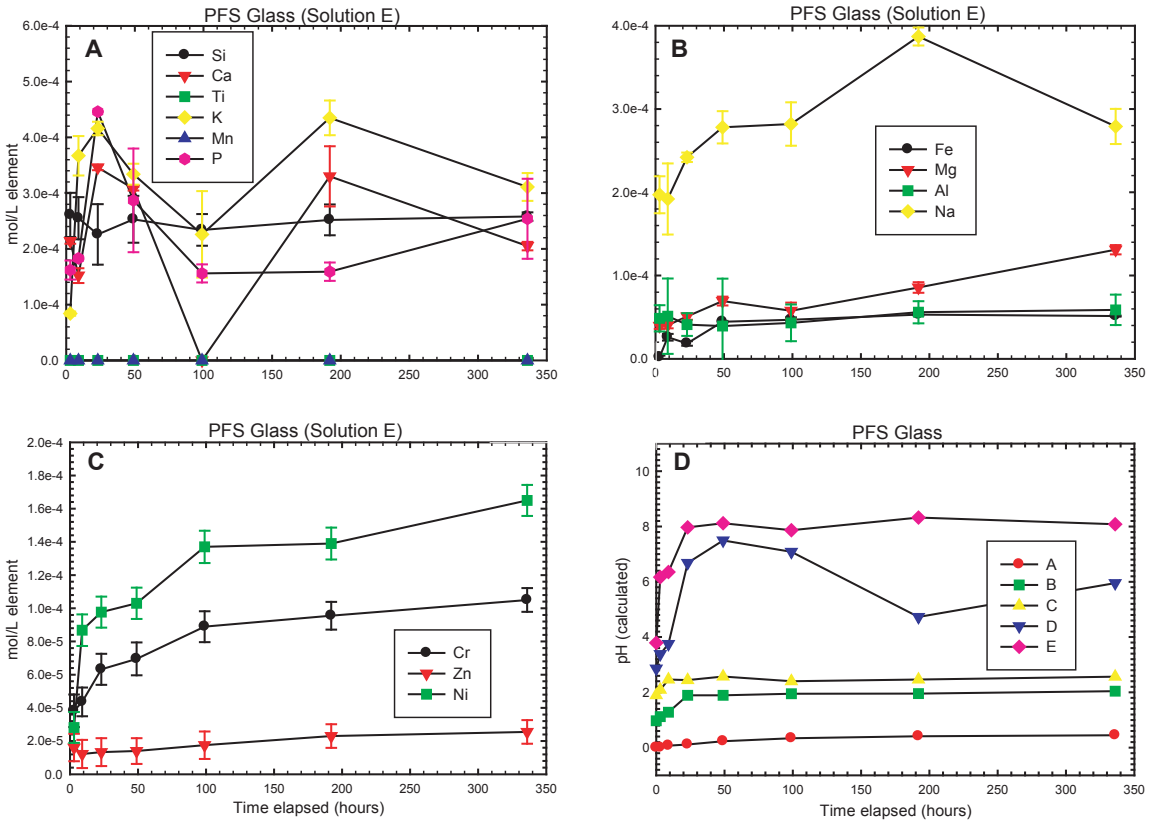

Figure B3. Major and trace element solution concentrations during reaction with PFS glass and (a through c) solution E. (d) Calculated pH values versus time.

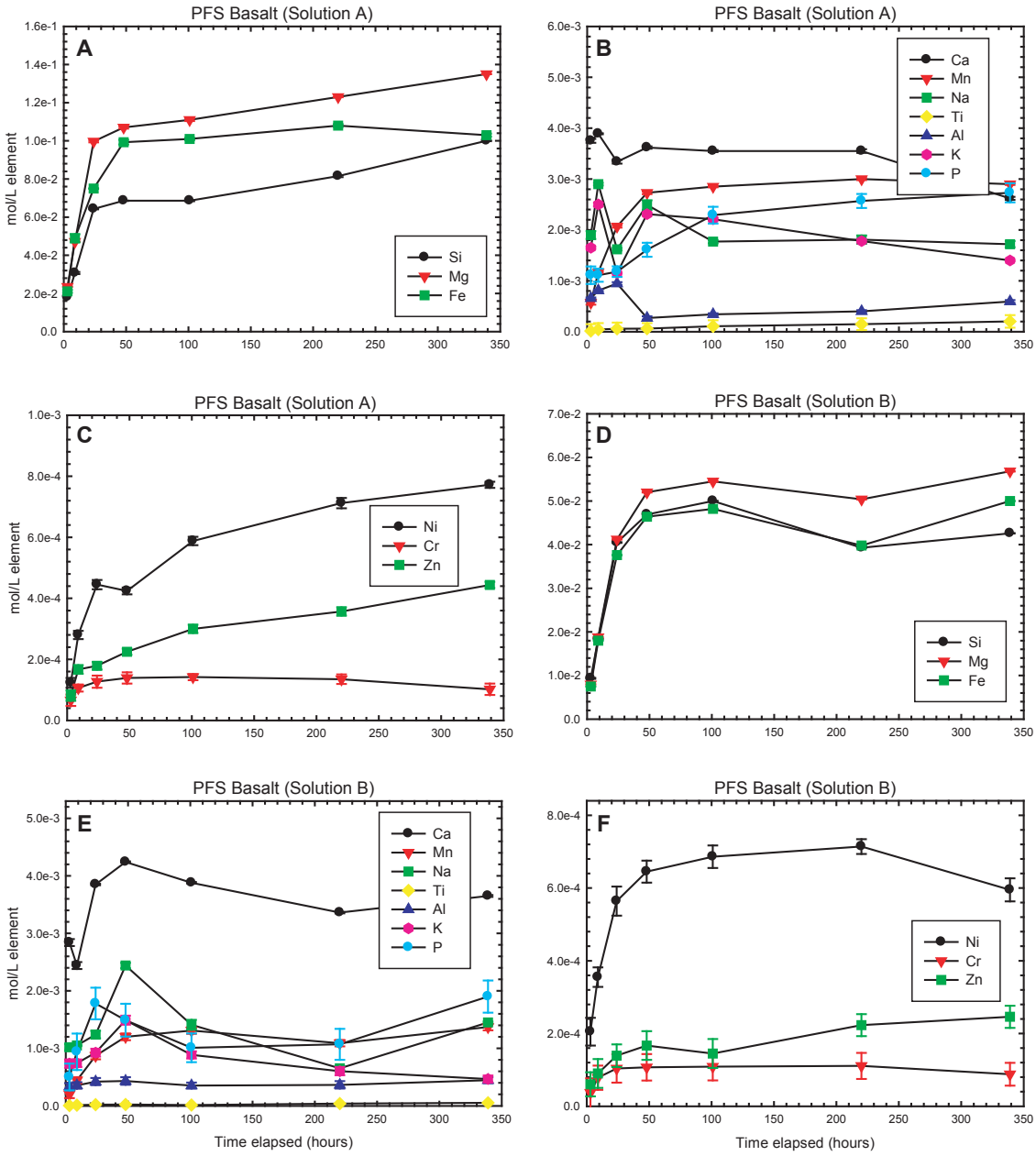

Figure B4. Major and trace element solution concentrations during reaction with PFS crystalline basalt and (a through c) solution A, and (d through f) solution B.

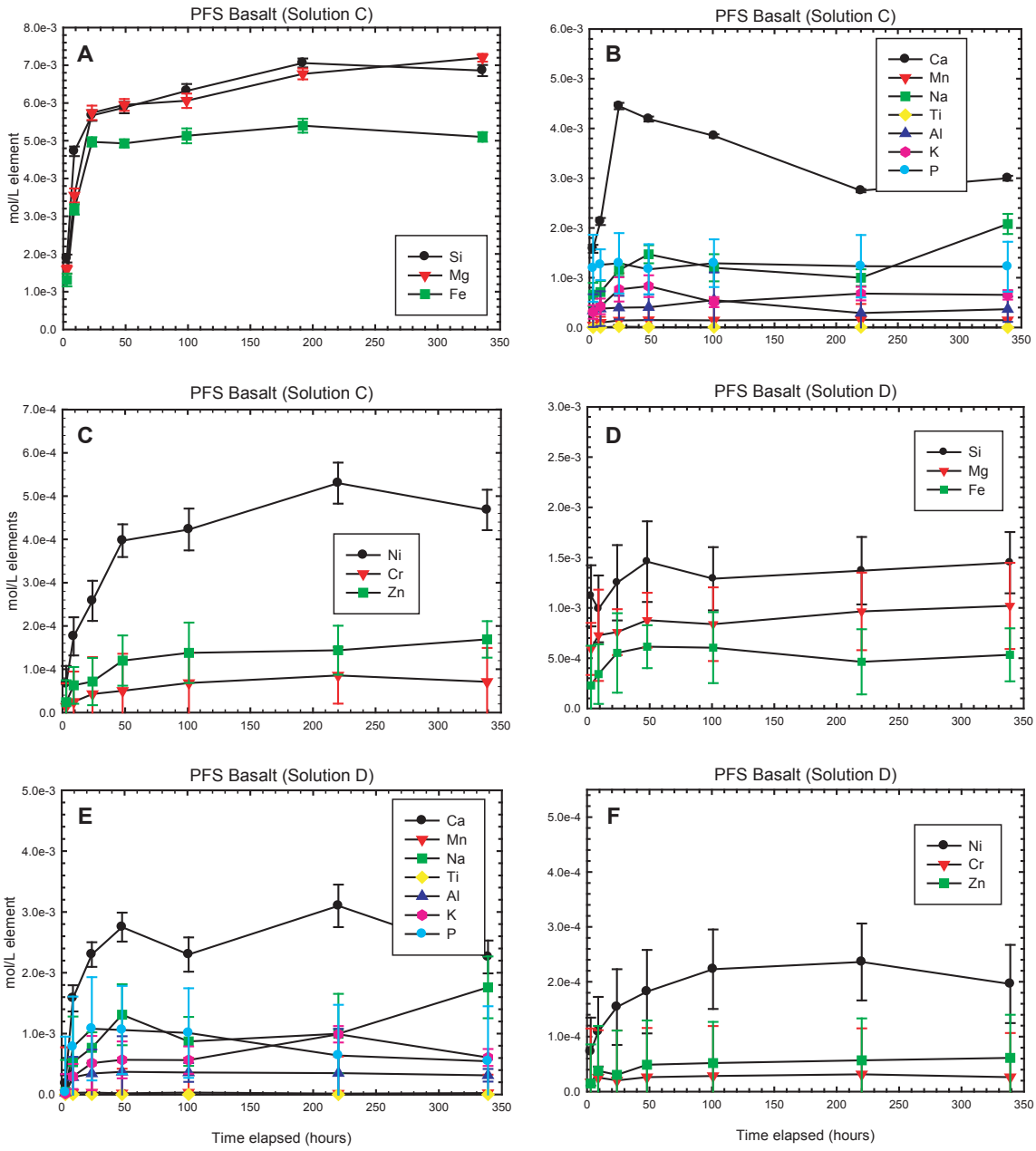

Figure B5. Major and trace element solution concentrations during reaction with PFS crystalline basalt and (a through c) solution C, and (d through f) solution D.

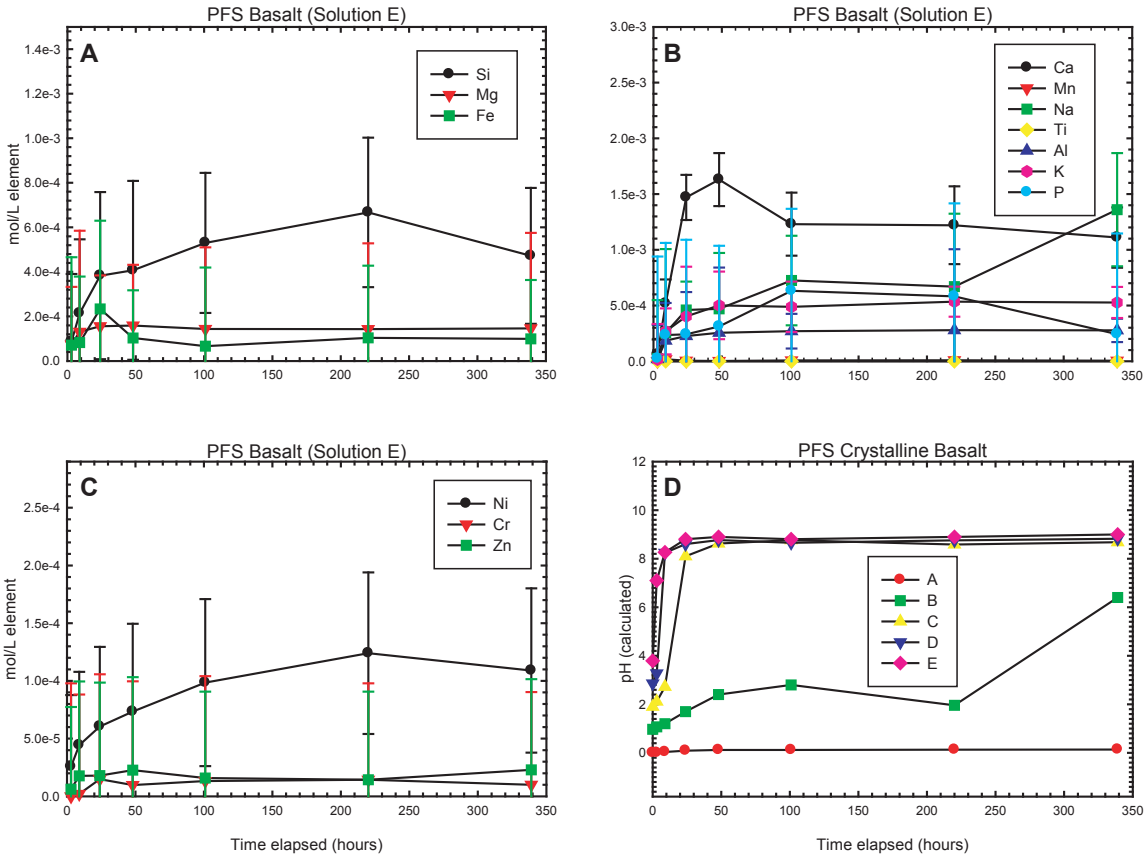

Figure B6. Major and trace element solution concentrations during reaction with PFS crystalline basalt and (a through c) solution E. (d) Calculated pH values during reaction.

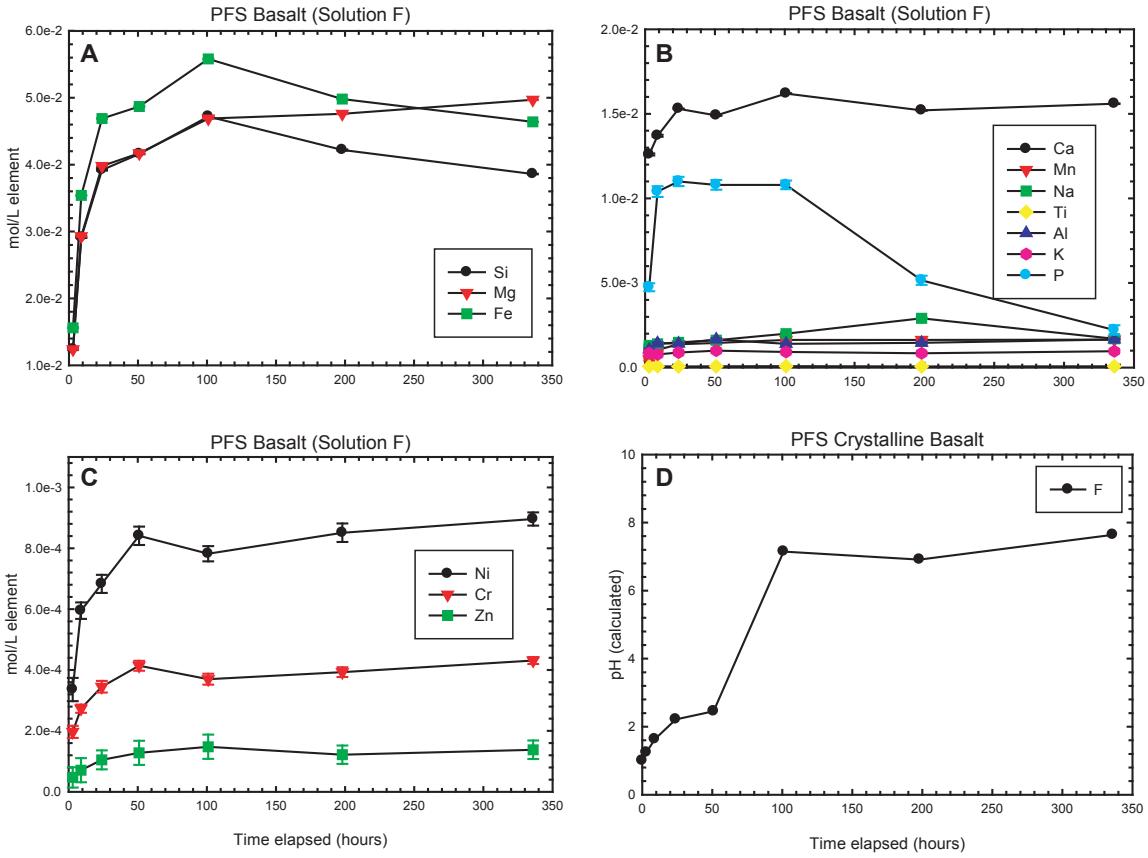

Figure B7. Major and trace element solution concentrations during reaction with PFS crystalline basalt with plagioclase and (a through c) solution F. (d) Calculated pH values during reaction.

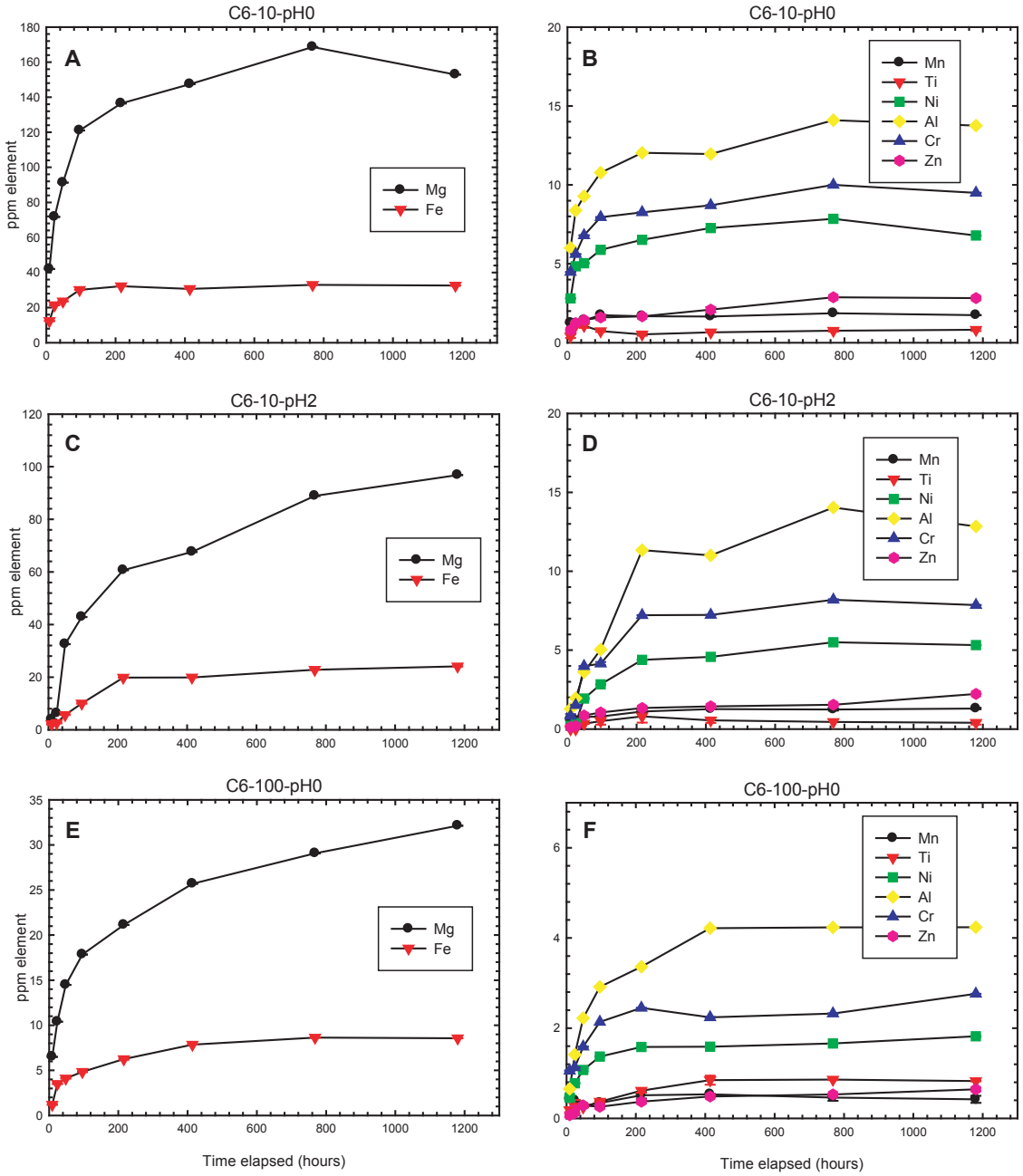

Figure B8. Major and trace element solution concentrations during reaction with C6 and (a and b) solution A and (c and d) solution B, both with a water to rock ratio of 10. C6 reacted with (e and f) solution A with a water to rock ratio of 100.

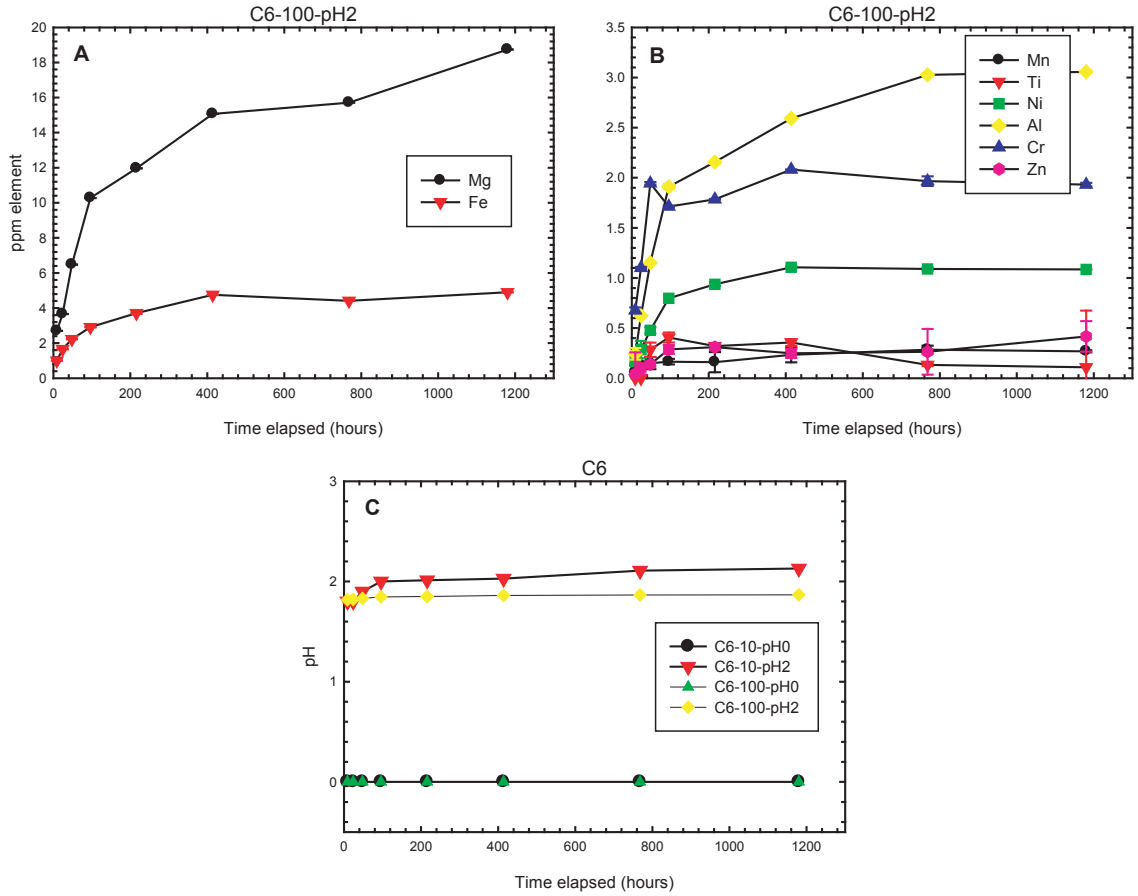

Figure B9. Major and trace element solution concentrations during reaction with C6 and (a and b) solutions B with a water to rock ratio of 100. (c) Calculated pH values during reactions.

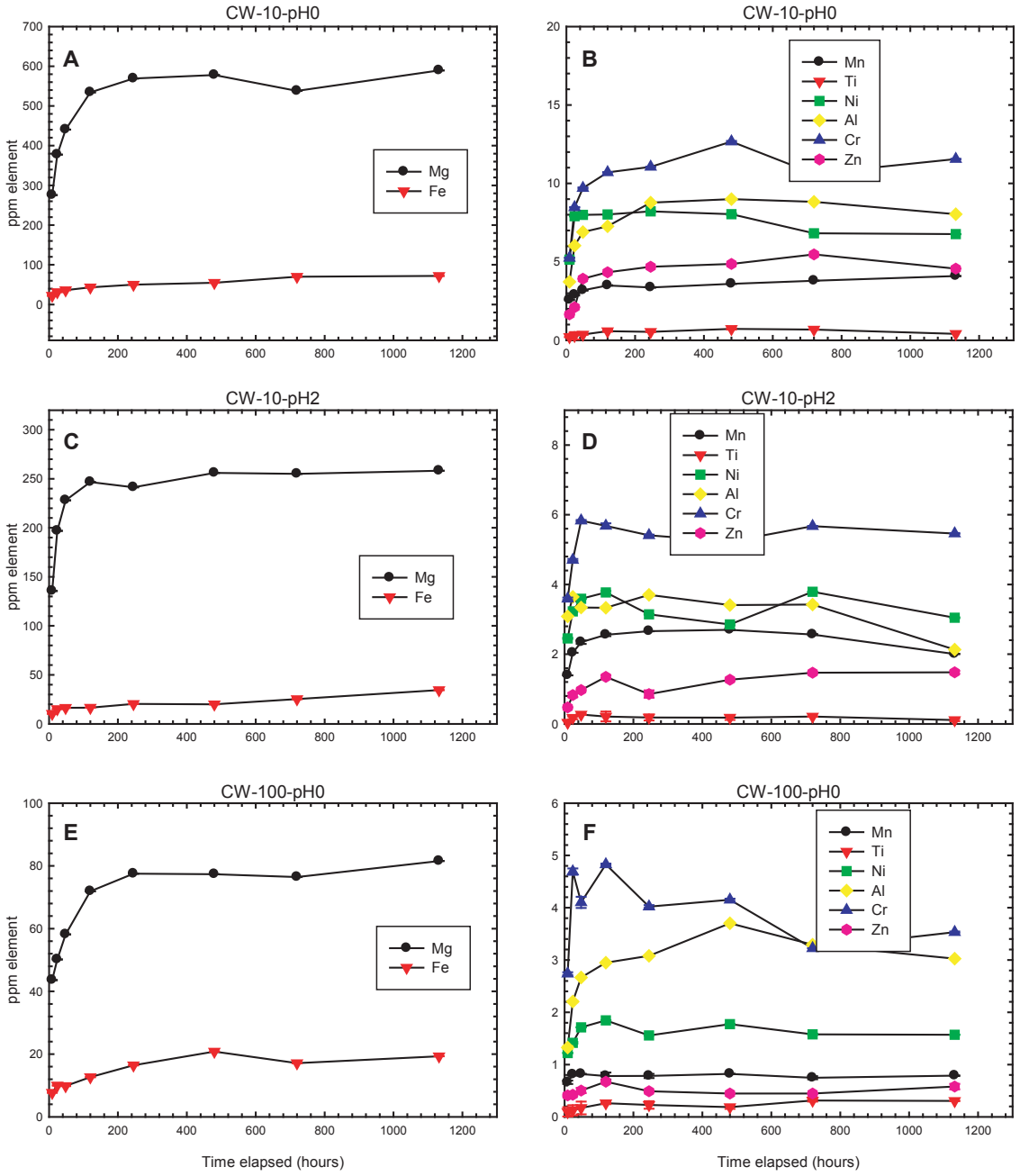

Figure B10. Major and trace element solution concentrations during reaction with CW and (a and b) solution A and (c and d) solution B, both with a water to rock ratio of 10. CW reacted with (e and f) solution A with a water to rock ratio of 100.

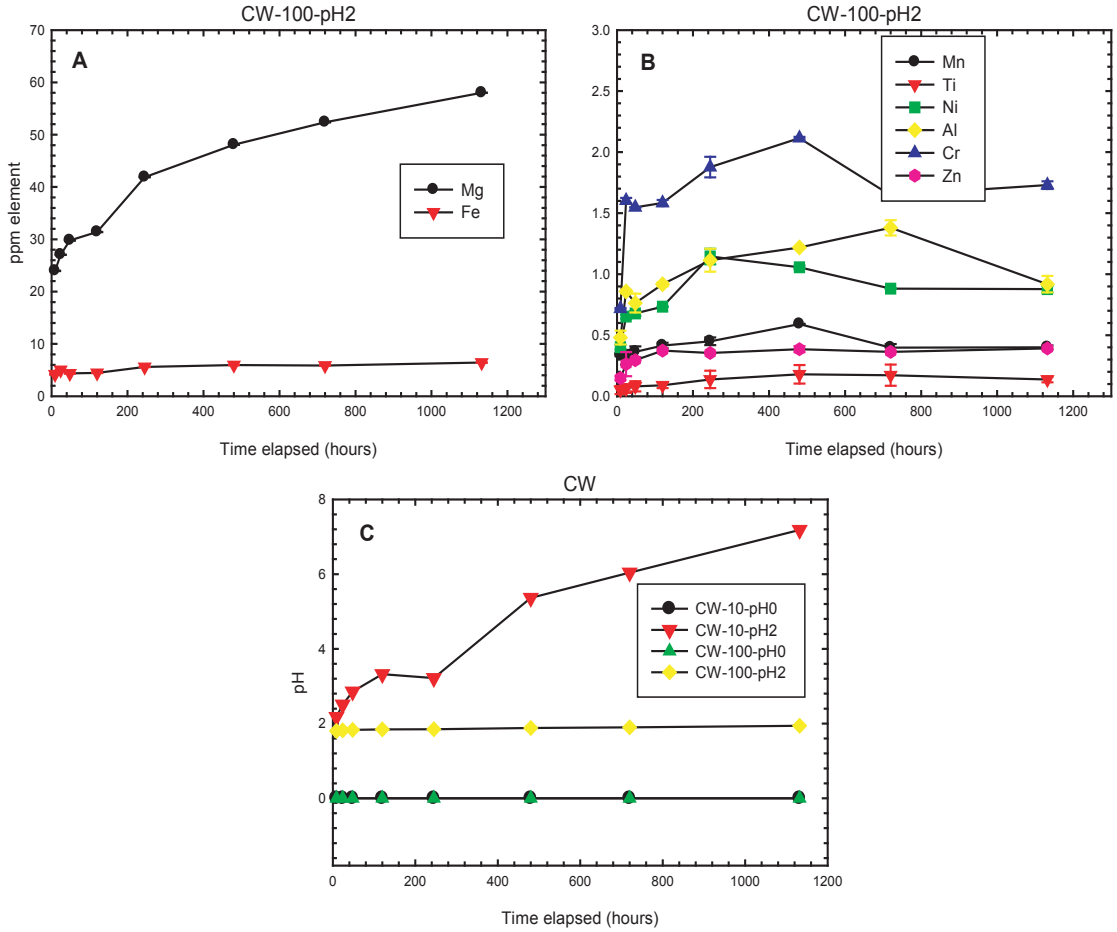

Figure B11. Major and trace element solution concentrations during reaction with CW and (a and b) solution B with a water to rock ratio of 100. (c) Calculated pH values during reaction.